An exact Riemann solver for one-dimensional multi-material elastic-plastic flows with Mie-Grüneisen equation of state without vacuum

Li Liu [1], Jun-bo Cheng [1,*]

[1] *Institute of Applied Physics and Computational Mathematics, Beijing 100094, China*

Abstract

In this paper, we present exact Riemann solvers for the Riemann problem and the half Riemann problem, respectively, for one-dimensional multi-material elastic-plastic flows with the Mie-Grüneisen equation of state(EOS), hypo-elastic constitutive model and the von Mises' yielding condition. We firstly analyze the Jacobian matrices in the elastic and plastic states, and then build the relations of different variables across different type of waves. Based on these formulations, an exact Riemann solver is constructed with totally thirty-six possible cases of wave structures. A large number of tests prove the rightness of the new exact Riemann solver. Moreover, an exact Riemann solver is also deduced for the half Riemann problem and its validity is tested by two examples.

Keywords: Elastic-plastic flows, Riemann problem, hypo-elastic model, exact Riemann solver, Mie-Grüneisen equation

1. Introduction

In this paper, an exact Riemann solver is built for one-dimensional multi-material elastic-plastic flows with the Mie-Grüneisen EOS, hypo-elastic constitutive model [1] and the von Mises' yielding condition.

The elastic-plastic flow is used to describe the deformation process of solid materials under strong dynamics loading, such as explosive or high-speed impact. The simulation of elastic-plastic flows has important application backgrounds, especially in the Implosion Dynamics weapon and Inertial Confine Fusion (ICF). The first try of simulating the elastic-plastic flows was given by Wilkins [1] in 1960s.

In the development history of hydrodynamic numerical methods, the exact Riemann solver has played a very important role as it not only can give a guide and reference to the construction of approximate Riemann solvers, but also can be used to determine the convergence and stability of numerical schemes. However, building the exact Riemann solver for 1D elastic-plastic flows is not easy. Comparing with the governing equations of 1D pure fluids, for 1D elastic-plastic flows, there are two more equations: a non-conservative constitutive equation and the von Mises yielding condition. The non-conservative character of the constitutive equation increases the difficulty in constructing Riemann solvers, while the von Mises yielding condition may

*Correspondence to: Junbo Cheng, Institute of Applied Physics and Computational Mathematics, Beijing 100094, China. E-mail: Cheng_junbo@iapcm.ac.cn

lead to more non-linear waves in the wave structure of Riemann solvers. Moreover, in a general way, the equation of state(EOS) for solid materials is more complex than that for pure fluids, which directly increases the difficulty in solving the Riemann problem.

For the elastic-plastic flow with the hypo-elastic constitutive model and the von Mises' yielding condition, some approximate Riemann solvers[2, 3, 4, 5] have been developed recently. However, for the exact Riemann solver, the research is relatively few, and focuses mainly on the problems with relatively simple constitutive models or relatively simple EOSs. For example, Garaizar [6] and Miller [7] introduced an exact Riemann solver for elastic or hyper-elastic materials, Gao and Liu [8, 9] firstly considered the yielding effect and developed an exact elastic-perfectly plastic solid Riemann solver. In Gao and Liu works [8, 9], a five-equation Eulerian governing system is constructed, and a complete list of sixty-four cases of wave type is presented.

In this paper, we construct an exact Riemann solver for the system of 1D elastic-plastic flows with the Mie-Grüneisen EOS, the hypo-elastic constitutive model and the von Mises' yielding condition. Although Gao and Liu [8, 9] have developed a comprehensive Riemann solver for 1D elastic-perfectly plastic solid, there are several notable differences and necessities of this paper. Firstly, a four-equation controlling system is considered in this paper, which is generally used in the simulation of one-dimensional elastic-plastic flows [10, 11]. In this four-equation system, the elastic and plastic states are treated with same equations of mass, momentum and energy but only different in deviatoric stress. While Gao and Liu [8, 9] use a five-equation system and treat the elastic and plastic states with totally different equations. Secondly, the same Mie-Grüneisen EOS is used in the elastic and plastic states, so the energy equation must be considered in both the elastic state and the plastic state. While in works [8, 9], the pressure is given as a function of the strain rate in the elastic state, so the energy equation is not considered in the elastic state. Besides, the Mie-Grüneisen EOS used in our work is more complex, and so, the process of resolving rarefaction waves is also different and of more difficulties.

This paper is organized as follows. In Section 2, we introduce the governing equations to be studied. In Section 3, the Riemann problem and the relations for every wave type (contact wave, shock wave and rarefaction wave) are derived. Then, the exact Riemann solver is given in Section 4. The half Riemann problem and its solver is introduced in Section 5. Some numerical examples are presented to validate our Riemann solvers in Section 6. Conclusions are shown in Section 7.

2. Governing equations

In this paper, the elastic energy is not included in the total energy. The exclusion of the elastic energy is usual for practical engineering problems [12] and is different from that in Ref.[2].

2.1. Motion equations

For a continuous one-dimensional homogeneous solid, the motion equations in the differential form are

$$\partial_t \mathbf{U} + \partial_x \boldsymbol{F}(\mathbf{U}) = 0,\ x \in\ \Omega \subset \mathbf{R},\ t > 0,$$

where

$$\mathbf{U} = \begin{bmatrix} \rho \\ \rho u \\ \rho E \end{bmatrix}, \quad \mathbf{F} = \begin{bmatrix} \rho u \\ \rho u^2 - \sigma \\ (\rho E - \sigma)u \end{bmatrix}, \tag{2.1}$$

ρ, u, σ and E are the density, velocity in $x-$direction, Cauchy stress and total energy per unit volume, respectively, E has the relation with the specific internal energy e as

$$E = e + \frac{1}{2}u^2, \tag{2.2}$$

$$\sigma = -p + s_{xx}, \tag{2.3}$$

where p and s_{xx} denote the hydrostatic pressure and the deviatoric stress in the $x-$ direction, respectively.

2.2. The equation of state (EOS)

The relation of the pressure with the density and the specific internal energy is gotten from the equation of state (EOS). In this paper, we consider the Mie-Grüneisen EOS,

$$p(\rho, e) = \rho_0 a_0^2 f(\eta) + \rho_0 \Gamma_0 e, \tag{2.4}$$

where $f(\eta) = \frac{(\eta-1)(\eta-\Gamma_0(\eta-1)/2)}{(\eta-s(\eta-1))^2}$, $\eta = \frac{\rho}{\rho_0}$, ρ_0, a_0, s and Γ_0 are the constant parameters of the Mie-Grüneisen EOS.

2.3. The constitutive relation

Hooke's law is used here to describe the relationship between the deviatoric stress and the strain,

$$\dot{s}_{xx} = 2\mu \left(\dot{\varepsilon}_x - \frac{1}{3}\frac{\dot{V}}{V} \right), \tag{2.5}$$

where μ is the shear modulus, V is the volume, and the dot means the material time derivative,

$$\dot{()} = \frac{\partial()}{\partial t} + u\frac{\partial()}{\partial t}, \tag{2.6}$$

and

$$\dot{\varepsilon}_x = \frac{\partial u}{\partial x}, \quad \frac{\dot{V}}{V} = \frac{\partial u}{\partial x}. \tag{2.7}$$

By using Eq.(2.7), Eq.(2.5) can be rewritten as

$$\frac{\partial s_{xx}}{\partial t} + u\frac{\partial s_{xx}}{\partial t} = \frac{4}{3}\mu\frac{\partial u}{\partial x}. \tag{2.8}$$

2.4. The yielding condition

The Von Mises' yielding condition is used here to describe the elastic limit. In one spatial dimension, the von Mises' yielding criterion is given by

$$|s_{xx}| \leq \frac{2}{3}Y_0, \tag{2.9}$$

where Y_0 is the yield strength of the material in simple tensions.

3. The Riemann problem

The Riemann problem for 1D time dependent elastic-plastic equations is given as follows:

$$\begin{cases} \partial_t \rho + \partial_x(\rho u) = 0, \\ \partial_t(\rho u) + \partial_x(\rho u^2 + p - s_{xx}) = 0, \\ \partial_t(\rho E) + \partial_x\left[(\rho E + p - s_{xx})u\right] = 0, \\ \begin{cases} \partial_t s_{xx} + u\partial_x s_{xx} - \frac{4}{3}\partial_x u = 0, \\ |s_{xx}| \leq \frac{2}{3}Y_0, \end{cases} \\ Q(x, t=0) = \begin{cases} Q_L, \text{ if } x < 0, \\ Q_R, \text{ if } x > 0, \end{cases} \end{cases} \tag{3.1}$$

where $Q = (\rho, \rho u, \rho E, s_{xx})^T$.

If the material is in the plastic state, the above forth equation can be simplified. Correspondingly, sonic velocity is different from that in the elastic state, which will be discussed in the following.

3.1. Elastic state

3.1.1. Jacobian matrix in elastic regions

For the Mie-Grüneisen EOS, if the material is not yielding,

$$|s_{xx}| < \frac{2}{3}Y_0,$$

the system (3.1) can be written as

$$\partial_t \mathbf{Q} + \mathbf{J}_e(\mathbf{Q})\partial_x \mathbf{Q} = 0,$$

where $Q = (\rho, \rho u, \rho E, s_{xx})$, and the Jacobian matrix is

$$\mathbf{J}_e(Q) = \begin{bmatrix} 0 & 1 & 0 & 0 \\ -u^2 + \frac{\partial p}{\partial \rho} + \Gamma(\frac{u^2}{2} - e) & u(2-\Gamma) & \Gamma & -1 \\ (\Gamma(\frac{u^2}{2} - e) - e - \frac{u^2}{2} + \frac{\sigma}{\rho} + \frac{\partial p}{\partial \rho})u & -\Gamma u^2 - \frac{\sigma}{\rho} + \frac{u^2}{2} + e & (1+\Gamma)u & -u \\ \frac{4}{3}\mu\frac{u}{\rho} & -\frac{4}{3}\mu\frac{1}{\rho} & 0 & u \end{bmatrix}, \tag{3.2}$$

where $\Gamma = \frac{\Gamma_0 \rho_0}{\rho}$.

The eigenvalues of $\mathbf{J}_e(\mathbf{Q})$ are given as

$$\lambda_1 = \lambda_2 = u, \quad \lambda_3 = u - c_e, \quad \lambda_4 = u + c_e,$$

where c_e means the sonic speed of the solid in the elastic state,

$$\begin{cases} c_e = \sqrt{a^2 - \dfrac{\rho_0}{\rho^2}\Gamma_0 s_{xx} + \dfrac{4}{3}\dfrac{\mu}{\rho}}, \\ a^2 = \dfrac{\partial p}{\partial \rho} + \dfrac{p}{\rho^2}\dfrac{\partial p}{\partial e} = a_0^2 \dfrac{\partial f}{\partial \eta} + \dfrac{p}{\rho^2}\rho_0 \Gamma_0. \end{cases} \tag{3.3}$$

Corresponding right eigenvectors are

$$r_1 = \begin{bmatrix} \frac{1}{b_1} \\ \frac{u}{b_1} \\ 0 \\ 1 \end{bmatrix}, \quad r_2 = \begin{bmatrix} -\frac{\Gamma}{b_1} \\ -\frac{\Gamma u}{b_1} \\ 1 \\ 0 \end{bmatrix}, \quad r_3 = \frac{1}{\phi^2} \begin{bmatrix} 1 \\ u - c_e \\ h - u c_e \\ \phi^2 \end{bmatrix}, \quad r_4 = \frac{1}{\phi^2} \begin{bmatrix} 1 \\ u + c_e \\ h + u c_e \\ \phi^2 \end{bmatrix}, \tag{3.4}$$

where

$$b_1 = \frac{\partial p}{\partial \rho} - \Gamma E, \quad h = E + \frac{p - s_{xx}}{\rho},$$

and

$$\phi^2 = a^2 - \frac{\rho_0}{\rho^2}\Gamma_0 s_{xx} - c_e^2 = -\frac{4\mu}{3}\frac{1}{\rho}.$$

3.1.2. Relations across the contact wave

For a system without molecular diffusion, there is no materials convecting across the contact wave or interface, so the velocities on two sides of the discontinuity are always equal. This can also be verified by eigenvectors in Eq.(3.4) and Eq.(3.51).

Use $\mathbf{Q}_L^*$ and $\mathbf{Q}_R^*$ to denote the two states connected by the contact wave in the solution, where $\mathbf{Q} = (\rho, u, p, s_{xx})$.

Thanks to Eq.(3.4), for the λ_1-wave we have

$$\frac{d\rho}{\frac{1}{b_1}} = \frac{d\rho u}{\frac{u}{b_1}} = \frac{d\rho E}{0} = \frac{d s_{xx}}{1}. \tag{3.5}$$

From above equations, we can easily deduce that

$$du = 0, \quad d(s_{xx} - p) = 0, \tag{3.6}$$

which means

$$u_L^* = u_R^*, \tag{3.7}$$

and

$$\sigma^*_{x,L} = \sigma^*_{x,R}, \tag{3.8}$$

where $()^*_L$ and $()^*_R$ denote $()$ in the regions of $\mathbf{Q}^*_L$ and $\mathbf{Q}^*_R$, respectively. Here we do not show the details of the derivation for a simple presentation.

Similarly, for the λ_2-wave one has

$$\frac{d\rho}{\frac{-\Gamma}{b_1}} = \frac{d\rho u}{\frac{-u\Gamma}{b_1}} = \frac{d\rho E}{1} = \frac{ds_{xx}}{0}. \tag{3.9}$$

From the above equations, we can easily deduce that

$$du = 0, \quad dp = 0, \quad ds_{xx} = 0, \tag{3.10}$$

which means

$$u^*_L = u^*_R, \tag{3.11}$$

$$p^*_L = p^*_R, \quad s^*_{xx,L} = s^*_{xx,R}. \tag{3.12}$$

From Eq.(3.12), we get that

$$\sigma^*_{x,L} = \sigma^*_{x,R}. \tag{3.13}$$

At last, for the λ_1 and λ_2 waves, one can find that the following two relations always hold:

$$u^*_L = u^*_R, \quad \sigma^*_{x,L} = \sigma^*_{x,R}. \tag{3.14}$$

For convenience, we define

$$s^* = u^*_L = u^*_R. \tag{3.15}$$

where s^* denotes the velocity of the contact wave.

3.1.3. Relations across rarefaction waves

Left-going rarefaction wave

Across the left wave associated with λ_3-wave, ($\lambda_3 = u - c_e$), we have

$$\frac{d\rho}{1} = \frac{d(\rho u)}{u - c_e} = \frac{d(\rho E)}{h - uc_e} = \frac{ds_{xx}}{-\frac{4\mu}{3}\frac{1}{\rho}}. \tag{3.16}$$

which leads to

$$\mathrm{d}u = -\frac{c_e}{\rho}\mathrm{d}\rho, \tag{3.17}$$

$$\mathrm{d}E = -\frac{\sigma + \rho u c_e}{\rho^2}d\rho, \tag{3.18}$$

$$\mathrm{d}s_{xx} = -\frac{4}{3}\frac{\mu}{\rho}d\rho. \tag{3.19}$$

Using (2.4), one can get

$$dE = de + udu. \tag{3.20}$$

Substituting (3.17) and (3.18) into the above equation yields

$$de = -\frac{\sigma}{\rho^2}d\rho = \frac{p - s_{xx}}{\rho^2}d\rho. \tag{3.21}$$

Thanks to (2.4), one can get

$$dp = \frac{\partial p}{\partial \rho}d\rho + \frac{\partial p}{\partial e}de = a_0^2\frac{\partial f}{\partial \eta}d\rho + \rho_0\Gamma_0 de, \tag{3.22}$$

Substituting (3.21) into the above equation yields

$$dp = \left(a_0^2\frac{\partial f}{\partial \eta} + \frac{p}{\rho^2}\rho_0\Gamma_0 - \frac{\rho_0}{\rho^2}\Gamma_0 s_{xx}\right)d\rho. \tag{3.23}$$

The above equation can be rewritten as a differential equation of $p(\rho)$

$$p'(\rho) - \lambda\frac{p}{\rho^2} = f_2(\rho), \tag{3.24}$$

where

$$\lambda = \rho_0\Gamma_0 \quad f_2(\rho) = a_0^2\frac{\partial f}{\partial \eta} - \lambda\frac{s_{xx}(\rho)}{\rho^2}. \tag{3.25}$$

By integrating (3.24) across the left rarefaction wave, the pressure can be solved out as

$$pe^{\frac{\lambda}{\rho}} - \int f_2(\rho)e^{\frac{\lambda}{\rho}}d\rho = \text{constant}. \tag{3.26}$$

Integrating (3.17) across the left rarefaction wave yields

$$u + \int \frac{c_e}{\rho}d\rho = \text{constant}. \tag{3.27}$$

Right-going rarefaction wave

Across the right wave associated with λ_4-wave, ($\lambda_3 = u + c_e$), we have

$$\frac{d\rho}{1} = \frac{d(\rho u)}{u + c_e} = \frac{d(\rho E)}{h + uc_e} = \frac{ds_{xx}}{-\frac{4\mu}{3}\frac{1}{\rho}}. \tag{3.28}$$

which leads to

$$\mathrm{d}u = \frac{c_e}{\rho}\mathrm{d}\rho, \tag{3.29}$$

$$\mathrm{d}E = -\frac{\sigma + \rho u c_e}{\rho^2} d\rho, \tag{3.30}$$

$$\mathrm{d}s_{xx} = -\frac{4}{3}\frac{\mu}{\rho} d\rho. \tag{3.31}$$

By using the same method as the left wave, one can get

$$pe^{\frac{\lambda}{\rho}} - \int f_2(\rho) e^{\frac{\lambda}{\rho}} d\rho = \text{constant}. \tag{3.32}$$

$$u - \int \frac{c_e}{\rho} d\rho = \text{constant}. \tag{3.33}$$

3.1.4. Relations across shock waves

Now we consider a shock wave moving with the speed of s. The data in front of the shock is $(\rho_1, u_1, p_1, s_{xx1})$ and that after the shock is $(\rho_2, u_2, p_2, s_{xx2})$.

We transform the equations to the frame of reference moving with the shock. The Rankine-Hugoniot conditions are given as

$$\rho_2(u_2 - s) = \rho_1(u_1 - s), \tag{3.34}$$

$$\rho_2 u_2(u_2 - s) = \rho_1 u_1(u_1 - s) + \sigma_2 - \sigma_1, \tag{3.35}$$

$$\rho_2 E_2(u_2 - s) = \rho_1 E_1(u_1 - s) + \sigma_2 u_2 - \sigma_1 u_1. \tag{3.36}$$

Substituting (3.34) into (3.35) yields

$$\rho_1(u_2 - u_1)(u_1 - s) = \sigma_2 - \sigma_1. \tag{3.37}$$

From (3.34), one has

$$u_1 - s = \frac{(u_1 - u_2)\rho_2}{\rho_2 - \rho_1}, \tag{3.38}$$

then substituting it into (3.37) yields

$$-t(u_2 - u_1)^2 = \sigma_2 - \sigma_1, \tag{3.39}$$

where $t = \frac{\rho_1\rho_2}{\rho_2 - \rho_1}$.

By using the same methods for (3.39), (3.36) can be written as

$$t(u_1 - u_2)(E_2 - E_1) = \sigma_2 u_2 - \sigma_1 u_1. \tag{3.40}$$

Because of $E = e + \frac{1}{2}u^2$, we can get

$$e_2 - e_1 = -\frac{\sigma_1 + \sigma_2}{2t}. \tag{3.41}$$

Using the EOS of Mie-Grüneisen (2.4), can get

$$e = c_0 p - c_1 f(\rho/\rho_0), \tag{3.42}$$

where $c_0 = \frac{1}{\rho_0 \Gamma_0}$ and $c_1 = \frac{a_0^2}{\Gamma_0}$. Put the above equation into (3.41), we can formulate the pressure p_2 in terms of ρ_2.

$$p_2 = \frac{2t(c_1 f(\rho_2/\rho_0) + e_1) - (\sigma_1 + s_{xx2})}{2tc_0 - 1}. \tag{3.43}$$

Thanks to (3.66), s_{xx2} can be written as

$$s_{xx2} = s_{xx1} - \frac{4}{3}\mu \ln(\frac{\rho_2}{\rho_1}). \tag{3.44}$$

Then, the Cauchy stress can be written as

$$\sigma_2 = -p_2 + s_{xx2}. \tag{3.45}$$

We can use (3.39) to solve the velocity after the shock

$$u_2 = \begin{cases} u_1 - \sqrt{\dfrac{\sigma_1 - \sigma_2}{t}} & \text{Left-going,} \\ u_1 + \sqrt{\dfrac{\sigma_1 - \sigma_2}{t}} & \text{Right-going.} \end{cases} \tag{3.46}$$

And the shock speed is given as

$$s = \frac{\rho_2 u_2 - \rho_1 u_1}{\rho_2 - \rho_1}. \tag{3.47}$$

3.2. Plastic state

When the material is yielding,

$$|s_{xx}| = \frac{2}{3} Y_0, \tag{3.48}$$

the equations of Riemann problem can be simplified as

$$\begin{cases} \partial_t \rho + \partial_x(\rho u) = 0, \\ \partial_t(\rho u) + \partial_x(\rho u^2 + p - s_{xx}) = 0, \\ \partial_t(\rho E) + \partial_x\left[(\rho E + p - s_{xx})u\right] = 0, \\ |s_{xx}| = \dfrac{2}{3} Y_0, \\ U(x, t=0) = \begin{cases} U_L, \text{ if } x < 0, \\ U_R, \text{ if } x > 0, \end{cases} \end{cases} \tag{3.49}$$

where $\mathbf{U} = (\rho, \rho u, \rho E)$.

3.2.1. Jacobian matrix in plastic regions

Motion equations of (3.49) can be written as

$$\partial_t \mathbf{U} + \mathbf{J}_p(\mathbf{U}) \partial_x \mathbf{U} = 0,$$

where the Jacobian matrix is

$$\mathbf{J}_p(\mathbf{U}) = \begin{bmatrix} 0 & 1 & 0 \\ -u^2 + \frac{\partial p}{\partial \rho} + \Gamma(\frac{u^2}{2} - e) & u(2-\Gamma) & \Gamma \\ (\Gamma(\frac{u^2}{2} - e) - e - \frac{u^2}{2} + \frac{\sigma}{\rho} + \frac{\partial p}{\partial \rho})u + \frac{u^2}{2} & -\Gamma u^2 - \frac{\sigma}{\rho} + e & (1+\Gamma)u \end{bmatrix}.$$

Eigenvalues of $\mathbf{J}_p(\mathbf{Q})$ are given as

$$\lambda_1 = u, \quad \lambda_2 = u - c_p, \quad \lambda_3 = u + c_p,$$

where c_p shows the sonic speed in the plastic state,

$$c_p = \sqrt{a^2 - \frac{\rho_0}{\rho^2} \Gamma_0 s_{xx}}. \tag{3.50}$$

The corresponding right eigenvectors are

$$r_1 = \begin{bmatrix} -\frac{\Gamma}{b_1} \\ -\frac{\Gamma u}{b_1} \\ 1 \end{bmatrix}, \quad r_2 = \frac{1}{h - u c_p} \begin{bmatrix} 1 \\ u - c_p \\ h - u c_p \end{bmatrix}, \quad r_3 = \frac{1}{h + u c_p} \begin{bmatrix} 1 \\ u + c_p \\ h + u c_p \end{bmatrix}. \tag{3.51}$$

Comparing Eq.(3.3) with Eq.(3.50), we notice that the sonic speed is not continuous between the elastic state and plastic state. As the shear modulus μ is always positive, the elastic wave runs always faster than the plastic wave.

3.2.2. Relations across the contact wave

According to the eigenvectors in Eq.(3.51), for the λ_1-wave ($\lambda_1 = u$), we have

$$\frac{d\rho}{\frac{-\Gamma}{b_1}} = \frac{d(\rho u)}{\frac{-u\Gamma}{b_1}} = \frac{d(\rho E)}{1}. \tag{3.52}$$

From the above equations, we can easily deduce that

$$du = 0, \quad dp = 0,$$

which means that

$$u_L^* = u_R^*, \quad p_L^* = p_R^*.$$

Because $s_{xxL}^* = s_{xxR}^*$, thanks to (2.3), one can get

$$\sigma_L^* = \sigma_R^*.$$

For convenience, we define

$$s^* = u_L^* = u_R^*.$$

3.2.3. Relations across rarefaction waves

Left-going rarefaction wave

Across the left wave associated with λ_2-wave, ($\lambda_2 = u - c_p$), we have

$$\frac{d\rho}{1} = \frac{d(\rho u)}{u - c_p} = \frac{d(\rho E)}{h - uc_p}. \tag{3.53}$$

Similar to Section 3.1.3, we can get the relations

$$pe^{\frac{\lambda}{\rho}} - \int f_2(\rho) e^{\frac{\lambda}{\rho}} d\rho = \text{constant}. \tag{3.54}$$

and

$$u + \int \frac{c_p}{\rho} d\rho = \text{constant}. \tag{3.55}$$

Right-going rarefaction wave

Across the right wave associated with λ_3-wave, ($\lambda_3 = u + c_p$), we have

$$\frac{d\rho}{1} = \frac{d(\rho u)}{u + c_p} = \frac{d(\rho E)}{h + uc_p}. \tag{3.56}$$

Similarly, we can get

$$pe^{\frac{\lambda}{\rho}} - \int f_2(\rho) e^{\frac{\lambda}{\rho}} d\rho = \text{constant}. \tag{3.57}$$

$$u - \int \frac{c_p}{\rho} d\rho = \text{constant}. \tag{3.58}$$

3.2.4. Relations across a shock wave

By using the same deducing process as Section 3.1.4, we can get the state after the shock wave:

$$s_{xx2} = s_{xx1}, \tag{3.59}$$

$$p_2 = \frac{2t(c_1 f(\rho_2/\rho_0) + e_1) - (\sigma_1 + s_{xx2})}{2tc_0 - 1}, \tag{3.60}$$

where $c_0 = \frac{1}{\rho_0 \Gamma_0}$, $c_1 = \frac{a_0^2}{\Gamma_0}$, $\sigma_2 = -p_2 + s_{xx2}$,

$$u_2 = \begin{cases} u_1 - \sqrt{\dfrac{\sigma_1 - \sigma_2}{t}} & \text{Left-going,} \\ u_1 + \sqrt{\dfrac{\sigma_1 - \sigma_2}{t}} & \text{Right-going.} \end{cases} \tag{3.61}$$

And the shock speed is given as

$$s = \frac{\rho_2 u_2 - \rho_1 u_1}{\rho_2 - \rho_1}. \tag{3.62}$$

3.3. A relation between ρ and s_{xx}

Thanks to (2.6), the equations of the density and the deviatoric stress in Eq.(3.1) can be written as

$$\frac{\partial u}{\partial x} = -\frac{1}{\rho}\frac{d\rho}{dt}, \tag{3.63}$$

and

$$\frac{ds_{xx}}{dt} = \frac{4}{3}\mu\frac{\partial u}{\partial x}. \tag{3.64}$$

Substituting (3.63) into (3.64) yields

$$\frac{ds_{xx}}{dt} = -\frac{4}{3}\mu\frac{1}{\rho}\frac{d\rho}{dt}. \tag{3.65}$$

Integrate the above equation from the data in front of a wave to the data behind the wave and perform some simple algebraic manipulations, one can get

$$s_{xx} + \frac{4}{3}\mu \ln(\rho) = \text{constant}. \tag{3.66}$$

Analyzing (3.66), one can find, $\frac{\partial s_{xx}}{\partial \rho} < 0$. So, if the material is compressed and ρ increases, s_{xx} will decrease; if the material is expanded and ρ decreases, s_{xx} will increase. According to the compressed or expanded process of the material, even if the initial material is in the plastic state, the material can be into a different state. With considering of the von Mises yielding condition, all cases are shown as follows:

1. If $s_{xx} = \frac{2}{3}Y^0$, initial material reaches the elastic limit. If the material is compressed so that $\rho_{plastic} > \rho^* > \rho$, one can get $|s^*_{xx}| < \frac{2}{3}Y^0$, the compressed material jumps from the plastic state to the

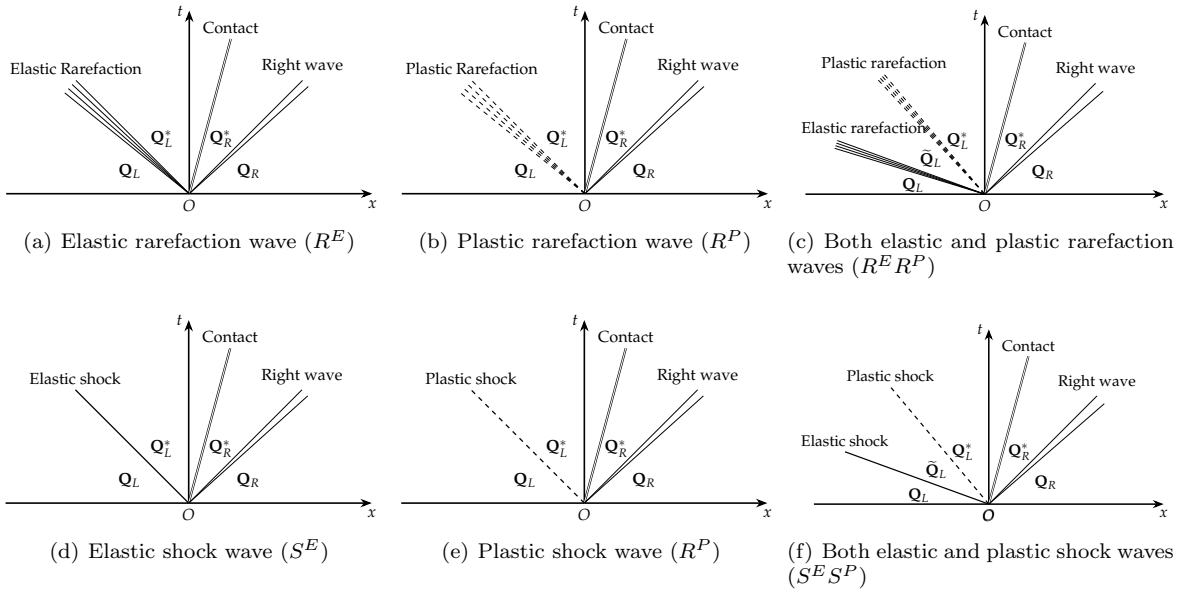

(a) Elastic rarefaction wave (R^E)

(b) Plastic rarefaction wave (R^P)

(c) Both elastic and plastic rarefaction waves ($R^E R^P$)

(d) Elastic shock wave (S^E)

(e) Plastic shock wave (R^P)

(f) Both elastic and plastic shock waves ($S^E S^P$)

Figure 1: The possible cases of Riemann solution structures in the left side.

elastic state. Here ρ and s_{xx} mean the initial density and deviatoric stress, respectively, $\rho_{plastic} = \rho e^{\left(-\frac{Y_0}{2\mu}+\frac{3s_{xx}}{4\mu}\right)}$, $()^*$ denotes the variable () of the compressed or expanded material.

2. If $s_{xx} = \frac{2}{3}Y^0$ and the material is compressed greatly so that $\rho_{plastic} < \rho^*$, $s^*_{xx} \leq -\frac{2}{3}Y^0$, the compressed material will jump from the positive plastic state to the negative plastic state. Here the positive or negative plastic state means $s_{xx} = \frac{2}{3}Y^0$ or $s_{xx} = -\frac{2}{3}Y^0$, respectively.

3. If $s_{xx} = \frac{2}{3}Y^0$ and the material is expanded, $s^*_{xx} > \frac{2}{3}Y^0$, the material is still in the positive plastic state.

4. If $s_{xx} = -\frac{2}{3}Y^0$ and the material is expanded so that $\rho_{plastic} < \rho^* < \rho$, one can get $|s^*_{xx}| < \frac{2}{3}Y^0$, the expanded material jumps from the plastic state to the elastic state.

5. If $s_{xx} = -\frac{2}{3}Y^0$ and the material is expanded greatly so that $\rho_{plastic} > \rho^*$, $s^*_{xx} \geq \frac{2}{3}Y^0$, the expanded material will jump from the negative plastic state to the positive plastic state.

6. If $s_{xx} = -\frac{2}{3}Y^0$ and the material is compressed, $s^*_{xx} < -\frac{2}{3}Y^0$, the material is still in the negative plastic state.

4. Exact Riemann solver

Now we consider the constructing details of the exact Riemann solver. For the Riemann problem in Section 3, there are 6×6 possible cases in the Riemann solution with different wave structures. The left six cases are shown in Fig.1. Here we remark that *we do not consider vacuum in building our exact Riemann solver.*

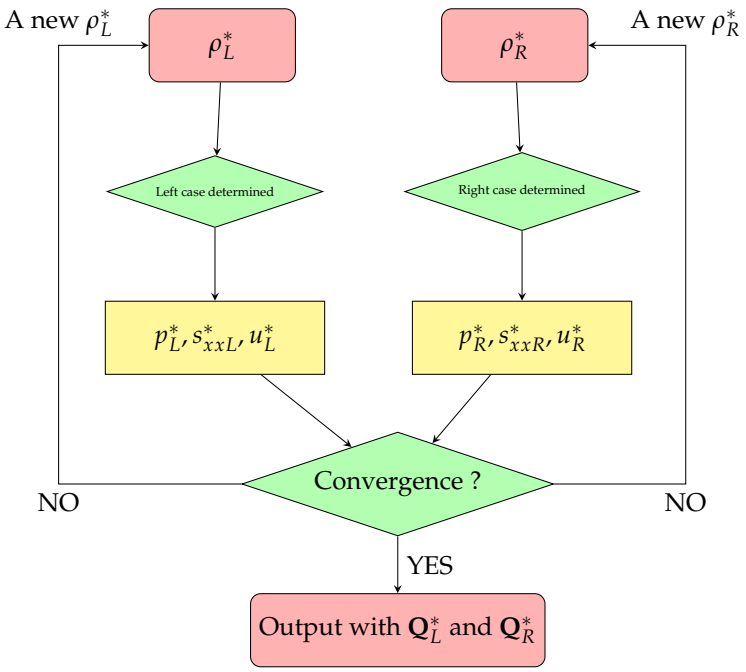

Figure 2: A flow chat of the Newton iteration process.

4.1. The solving process

From Section 3, we can find that all variables can be formulated in terms of the density. So we define functions f_u and f_σ:

$$\begin{cases} f_u(\rho_L^*, \rho_R^*, \mathbf{Q}_L, \mathbf{Q}_R) = u_L^*(\rho_L^*, \mathbf{Q}_L) - u_R^*(\rho_R^*, \mathbf{Q}_R), \\ f_\sigma(\rho_L^*, \rho_R^*, \mathbf{Q}_L, \mathbf{Q}_R) = \sigma_L^*(\rho_L^*, \mathbf{Q}_L) - \sigma_R^*(\rho_R^*, \mathbf{Q}_R). \end{cases} \tag{4.1}$$

By using the relations across the contact wave in Section 3.1.2 and Section 3.2.2, we can get

$$\begin{cases} f_u(\rho_L^*, \rho_R^*, \mathbf{Q}_L, \mathbf{Q}_R) = u_L^*(\rho_L^*, \mathbf{Q}_L) - u_R^*(\rho_R^*, \mathbf{Q}_R) = 0, \\ f_\sigma(\rho_L^*, \rho_R^*, \mathbf{Q}_L, \mathbf{Q}_R) = \sigma_L^*(\rho_L^*, \mathbf{Q}_L) - \sigma_R^*(\rho_R^*, \mathbf{Q}_R) = 0. \end{cases} \tag{4.2}$$

Obviously, this system is uniquely solvable, but we can not get the analytical solution of (4.2). We have to use an iteration procedure to solve (4.2) and the solving process is shown in Fig.2. The details are introduced in the following.

Initial:

The initial densities are given as

$$\rho_{L(1)}^* = \frac{\rho_L + \rho_R}{2} \quad \rho_{R(1)}^* = \frac{\rho_L + \rho_R}{2}. \tag{4.3}$$

Iterations begin:

Step 1 Determining the case of the wave structure:

Given $\rho^*_{L(k)}$ and $\rho^*_{R(k)}$ in the k-th iteration step, we can use the method introduced in Section 4.2 to determine the case of wave structure of this Riemann problem. In the procedure for solving the Riemann problem, the subscript (k) means the variable in the k-th iteration step.

Step 2 Evaluating $f_{u(k)}$ and $f_{\sigma(k)}$:

After determining the structures case, we need to solve Cauchy stresses and velocities in regions $\mathbf{Q}^*_L$ and $\mathbf{Q}^*_R$ and the details are given in Section 4.4.

Step 3 Evaluating the derivatives of $f_{u(k)}$ and $f_{\sigma(k)}$.

The derivatives of $f_{u(k)}$ and $f_{\sigma(k)}$ are given as

$$\frac{\partial f_{u(k)}}{\partial \rho^*_{L(R)}} = \frac{f_{u(k)} - f_{u(k-1)}}{\rho^*_{L(R)(k)} - \rho_{L(R)(k-1)}}, \quad \frac{\partial f_{\sigma(k)}}{\partial \rho^*_{L(R)}} = \frac{f_{\sigma(k)} - f_{\sigma(k-1)}}{\rho^*_{L(R)(k)} - \rho_{L(R)(k-1)}}. \tag{4.4}$$

At the first step, we use a simple numerical difference method to evaluate

$$\frac{\partial f_{u(1)}}{\partial \rho^*_{L(R)}} = \frac{f_u(\rho^*_{L(R)(1)} + \Delta\rho) - f_u(\rho^*_{L(R)(1)})}{\Delta\rho_{L(R)(1)}}, \quad \frac{\partial f_{u(1)}}{\partial \rho^*_{L(R)}} = \frac{f_u(\rho^*_{L(R)(1)} + \Delta\rho) - f_u(\rho^*_{L(R)(1)})}{\Delta\rho_{L(R)(1)}}, \tag{4.5}$$

where $\Delta\rho$ is a small quantity, here we define it as

$$\Delta\rho = \frac{\rho^*_{L(R)(1)}}{100}. \tag{4.6}$$

Step 4 Evaluating $\rho^*_{L(k+1)}$ and $\rho^*_{R(k+1)}$:

$$\begin{bmatrix} \rho^*_{L(k+1)} \\ \rho^*_{R(k+1)} \end{bmatrix} = \begin{bmatrix} \rho^*_{L(k)} \\ \rho^*_{R(k)} \end{bmatrix} - \begin{bmatrix} \frac{\partial f_{u(k)}}{\partial \rho^*_L} & \frac{\partial f_{u(k)}}{\partial \rho^*_R} \\ \frac{\partial f_{\sigma(k)}}{\partial \rho^*_L} & \frac{\partial f_{\sigma(k)}}{\partial \rho^*_R} \end{bmatrix}^{-1} \begin{bmatrix} f_{u(k)} \\ f_{\sigma(k)} \end{bmatrix} \tag{4.7}$$

Step 5 Convergence test:

The iteration is convergent if

$$\mathrm{CHA} \leq \mathrm{TOL}, \tag{4.8}$$

where

$$\mathrm{CHA} = \max\left[\frac{|\rho^*_{L(k+1)} - \rho^*_{L,(k)}|}{\frac{1}{2}|\rho^*_{L(k+1)} + \rho^*_{L(k)}|}, \frac{|\rho^*_{R(k+1)} - \rho^*_{R,(k)}|}{\frac{1}{2}|\rho^*_{R(k+1)} + \rho^*_{R(k)}|}, |f_u|, |f_\sigma| \right], \tag{4.9}$$

$$\mathrm{TOL} = 10^{-4}.$$

If not, go to Step 1 and continue the iteration procedure until convergent. Numerical examples show, after 2-4 iterations, the condition (4.8) is satisfied.

Iterations end

Table 4.1: The condition of cases classification.

$\hat{\rho^*} < \rho$	$\hat{s}_{xx} < \frac{2}{3}Y_0$	$s_{xx} = \frac{2}{3}Y_0$ and $\hat{s}_{xx} \geq \frac{2}{3}Y_0$	other
	Case a: R^E	Case b: R^P	Case c: $R^E R^P$
$\hat{\rho^*} > \rho$	$\hat{s}_{xx} > -\frac{2}{3}Y_0$	$s_{xx} = -\frac{2}{3}Y_0$ and $\hat{s}_{xx} \leq -\frac{2}{3}Y_0$	other
	Case d: S^E	Case e: S^P	Case f: $S^E S^P$

4.2. Determining the case of structures

Given the value of density $\rho^*_{L(R)}$, we can distinguish the non-linear wave is a shock or rarefaction wave. This is done easily by comparing $\rho^*_{L(R)}$ with $\rho_{L(R)}$, the subscript $_{L(R)}$ means in the left(right) side of the contact wave.

$$\begin{cases} \text{a rarefaction wave:} & \text{if } \rho_{L(R)} > \rho^*_{L(R)}, \\ \text{a shock wave:} & \text{if } \rho_{L(R)} < \rho^*_{L(R)}. \end{cases} \tag{4.10}$$

Thanks to (3.66), the deviatoric stress can be evaluated as

$$\hat{s}_{xxL(R)} = -\frac{4}{3}\mu \ln\left(\frac{\rho^*_{L(R)}}{\rho_{L(R)}}\right) + s_{xxL(R)}. \tag{4.11}$$

According to the values of initial and evaluated deviatoric stresses in (4.11) in one side of the contact wave, the non-linear wave in this side may be:

$$\begin{cases} \text{an elastic rarefaction} & \text{if } \hat{s}_{xxL(R)} < \frac{2}{3}Y^0, \\ \text{a plastic rarefaction} & \text{if } s_{xxL(R)} = \frac{2}{3}Y^0 \text{ and } \hat{s}_{xxL(R)} \geq \frac{2}{3}Y_0, \\ \text{an elastic rarefaction and a following plastic rarefaction} & \text{if } s_{xxL(R)} < \frac{2}{3}Y_0 \text{ and } \hat{s}_{xxL(R)} \geq \frac{2}{3}Y_0, \\ \text{an elastic shock} & \text{if } \hat{s}_{xxL(R)} > -\frac{2}{3}Y_0, \\ \text{a plastic shock} & \text{if } s_{xxL(R)} = -\frac{2}{3}Y_0 \text{ and } \hat{s}_{xxL(R)} \leq -\frac{2}{3}Y_0, \\ \text{an elastic shock and a following plastic shock} & \text{if } s_{xxL(R)} > -\frac{2}{3}Y_0 \text{ and } \hat{s}_{xxL(R)} \leq -\frac{2}{3}Y_0. \end{cases} \tag{4.12}$$

Combining (4.10) and (4.12), we can find, in any side of the wave structures of this Riemann problem, there are six cases showed in Table 4.1, where capital letters "S" and "R" mean the shock and rarefaction wave, respectively; superscript letters "E" and "P" indicate the elastic and plastic state of a wave, respectively. Otherwise, the subscript L or R are omitted for simplification.

4.3. Evaluating states in middle regions ($\tilde{\mathbf{Q}}_L$ and $\tilde{\mathbf{Q}}_R$)

Cases (R^E, R^P, S^E and S^P)

For cases (R^E, R^P, S^E and S^P) in Fig.1, the material is totally yielding or totally not yielding, there is

no midlle state $\tilde{\mathbf{Q}}_{L(R)}$. For expression convenience, we let

$$(\tilde{\rho}_{L(R)}, \tilde{u}_{L(R)}, \tilde{p}_{L(R)}, \tilde{s}_{xx}) = (\rho_{L(R)}, u_{L(R)}, p_{L(R)}, s_{xxL(R)}), \tag{4.13}$$

Case $(R^E R^P)$

Using the methods introduced in the Section (3.1.3), we can easily deduce the formulation of all unknown variables after the rarefaction wave. Here we do not show the details of the deduction.

For the case $(R^E R^P)$, after the elastic rarefaction wave, the deviatoric stress achieves the elastic limit. Thanks to (4.10) and (4.12), one can easily deduce that

$$\tilde{s}_{xxL(R)} = \frac{2}{3} Y_0.$$

By using (3.66), the density in $\tilde{\mathbf{Q}}_{L(R)}$ is given as

$$\tilde{\rho}_{L(R)} = \rho_{L(R)} \exp\left(-\frac{Y_0}{2\mu} + \frac{3 s_{xxL(R)}}{4\mu}\right).$$

From (3.26) and (3.32), for the case $(R^E R^P)$, the pressure is rearranged as

$$\tilde{p}_{L(R)} = p_{L(R)} e^{\frac{\lambda}{\rho_{L(R)}} - \frac{\lambda}{\tilde{\rho}_{L(R)}}} + e^{-\frac{\lambda}{\tilde{\rho}_{L(R)}}} \int_{\rho_{L(R)}}^{\tilde{\rho}_{L(R)}} f_2(x) e^{\frac{\lambda}{x}} dx, \tag{4.14}$$

where

$$\lambda = \rho_0 \Gamma_0 \quad f_2(\rho) = a_0^2 \frac{\partial f}{\partial \eta} - \lambda \frac{s_{xx}(\rho)}{\rho^2}, \; s_{xx}(\rho) = -\frac{4}{3}\mu \ln\left(\frac{\rho}{\rho_{L(R)}}\right) + s_{xxL(R)}.$$

Thanks to (3.27) and (3.33), for the rarefaction wave case $(R^E R^P)$, the velocity is given as

$$\tilde{u}_{L(R)} = \begin{cases} u_L - \displaystyle\int_{\rho_L}^{\tilde{\rho}_{L(R)}} \frac{c_e(x)}{x} dx & \text{for the left-going rarefaction wave,} \\ u_R + \displaystyle\int_{\rho_R}^{\tilde{\rho}_{L(R)}} \frac{c_e(x)}{x} dx & \text{for the right-going rarefaction wave,} \end{cases} \tag{4.15}$$

where the sonic speed is given as

$$c_e(\rho) = \sqrt{a_0^2 \frac{\partial f}{\partial \eta} + \frac{p(\rho)}{\rho^2}\rho_0\Gamma_0 - \frac{\rho_0}{\rho^2}\Gamma_0 s_{xx}(\rho) + \frac{4}{3}\frac{\mu}{\rho}}.$$

Remark 1: In (4.14) and (4.15), there are two integral terms. Obviously, because of the complexity of the EOS, we can not get the exact integral values. We have to use the numerical methods to approximate the two integral terms with high order accuracy. The approximation methods are introduced in the Appendix A.

Case $(S^E S^P)$

Using the methods introduced in the Section (3.1.4), we can easily deduce the formulation of all unknown variables in $\tilde{\mathbf{Q}}_{L(R)}$. In order to shorten the length of our paper, we do not show the details of the deduction.

For the case $(S^E S^P)$, after the elastic shock wave, the deviatoric stress achieves the elastic limit. So, by using (4.10) and (4.12), one can easily deduce that

$$\tilde{s}_{xxL(R)} = -\frac{2}{3}Y_0.$$

From (3.66), after the elastic shock wave, the density in $\tilde{\mathbf{Q}}_{L(R)}$ is given as

$$\tilde{\rho}_{L(R)} = \rho_{L(R)}\exp\left(\frac{Y_0}{2\mu} + \frac{3s_{xxL(R)}}{4\mu}\right).$$

By using (3.43), the pressure can be solved as

$$\tilde{p}_{L(R)} = \frac{2t(c_1 f(\tilde{\rho}_{L(R)}/\rho_0) + e_{L(R)}) - (\sigma_{L(R)} + \tilde{s}_{xxL(R)})}{2tc_0 - 1}, \tag{4.16}$$

where $c_0 = \frac{1}{\rho_0\Gamma_0}$, $c_1 = \frac{a_0^2}{\Gamma_0}$ and $t = \frac{\rho_{L(R)}\tilde{\rho}_{L(R)}}{\tilde{\rho}_{L(R)} - \rho_{L(R)}}$.

Thanks to (3.46), the velocity can be written as

$$\begin{cases} \tilde{u}_L = u_L - \sqrt{\frac{\sigma_L - \tilde{\sigma}_L}{t}}, \\ \tilde{u}_R = u_R + \sqrt{\frac{\sigma_R - \tilde{\sigma}_R}{t}}, \end{cases} \tag{4.17}$$

where

$$\tilde{\sigma}_{L(R)} = -\tilde{p}_{L(R)} + \tilde{s}_{xxL(R)}. \tag{4.18}$$

4.4. Evaluating states in regions $\mathbf{Q}_L^*$ *and* $\mathbf{Q}_R^*$

Rarefaction wave cases $(R^E$***,*** R^P ***and*** $R^E R^P)$

For the three rarefaction wave cases, thanks to (3.66) and (3.48), s_{xx} in $\mathbf{Q}_L^*$ and $\mathbf{Q}_R^*$ are

$$s^*_{xxL(R)} = \begin{cases} -\frac{4}{3}\mu\ln\left(\frac{\rho^*_{L(R)}}{\tilde{\rho}_{L(R)}}\right) + s_{xxL(R)} & \text{for case } (R^E), \\ \frac{2}{3}Y_0 & \text{for cases } (R^P \text{ and } R^E R^P). \end{cases}$$

From (4.14), the pressure in the star region is

$$p^*_{L(R)} = \tilde{p}_{L(R)} e^{\frac{\lambda}{\rho_{L(R)}} - \frac{\lambda}{\rho}} + e^{-\frac{\lambda}{\rho^*_{L(R)}}} \int_{\tilde{\rho}_{L(R)}}^{\rho^*_{L(R)}} f_2(x) e^{\frac{\lambda}{x}} dx, \tag{4.19}$$

where

$$\lambda = \rho_0\Gamma_0 \quad f_2(\rho) = a_0^2\frac{\partial f}{\partial \eta} - \lambda\frac{s_{xx}(\rho)}{\rho^2},\ s_{xx}(\rho) = -\frac{4}{3}\mu\ln\left(\frac{\rho}{\rho_{L(R)}}\right) + s_{xxL(R)}.$$

By Equations (3.27) and (3.33) the velocity in regions $\mathbf{Q}_L^*$ and $\mathbf{Q}_R^*$ can be written as

$$u_{L(R)}^* = \begin{cases} \tilde{u}_L - \displaystyle\int_{\rho_L}^{\rho_{L(R)}^*} \frac{c(x)}{x} dx, \\ \tilde{u}_R + \displaystyle\int_{\rho_R}^{\rho_{L(R)}^*} \frac{c(x)}{x} dx, \end{cases} \tag{4.20}$$

where

$$c(\rho) = \begin{cases} \sqrt{a_0^2 \dfrac{\partial f}{\partial \eta} + \dfrac{p(\rho)}{\rho^2}\rho_0\Gamma_0 - \dfrac{\rho_0}{\rho^2}\Gamma_0 s_{xx}(\rho) + \dfrac{4}{3}\dfrac{\mu}{\rho}} & \text{for case } (R^E), \\ \sqrt{a_0^2 \dfrac{\partial f}{\partial \eta} + \dfrac{p(\rho)}{\rho^2}\rho_0\Gamma_0 - \dfrac{\rho_0}{\rho^2}\Gamma_0 s_{xx}(\rho)} & \text{for cases } (R^P \text{ and } R^E R^P). \end{cases}$$

Remark 2: Just like **Remark 1**, we have to use numerical integral methods introduced in the Appendix A to evaluate the integral terms in (4.19) and (4.20).

Shock wave cases (S^E, S^P and $S^E S^P$)

For shock wave cases, the deviatoric stresses in $\mathbf{Q}_L^*$ and $\mathbf{Q}_R^*$ are given as

$$s_{xx}(\rho) = \begin{cases} -\dfrac{4}{3}\mu \ln\left(\dfrac{\rho}{\tilde{\rho}_{L(R)}}\right) + \tilde{s}_{xxL(R)}, & \text{for case } (S^E), \\ -\dfrac{2}{3}Y_0, & \text{for cases (} S^P \text{ and } S^E S^P). \end{cases}$$

(3.43) gives direct expression for the the pressure in the star region as

$$p_{L(R)}^* = \frac{2t\left(c_1 f(\rho_{L(R)}^*/\rho_0) + \tilde{e}_{L(R)}\right) - \left(\tilde{\sigma}_{L(R)} + s_{xx}(\rho_{L(R)}^*)\right)}{2tc_0 - 1},$$

where $c_0 = \frac{1}{\rho_0\Gamma_0}$, $c_1 = \frac{a_0^2}{\Gamma_0}$ and $t = \frac{\rho_{L(R)}^* \tilde{\rho}_{L(R)}}{\rho_{L(R)}^* - \tilde{\rho}_{L(R)}}$.

Thanks to (3.46), the velocities in $\mathbf{Q}_L^*$ and $\mathbf{Q}_R^*$ are

$$u_{L(R)}^* = \begin{cases} \tilde{u}_L - \sqrt{\dfrac{\tilde{\sigma}_L - \sigma_{L(R)}^*}{t}} & \text{for the left-going shock wave,} \\ \tilde{u}_R + \sqrt{\dfrac{\tilde{\sigma}_R - \sigma_{L(R)}^*}{t}} & \text{for the right-going shock wave,} \end{cases}$$

where $\sigma_{L(R)}^* = -p_{L(R)}^* + s_{xxL(R)}^*$.

5. Half Riemann problem and its solver

Sometimes we need to analyse a half Riemann problem with a given velocity or Cauchy stress. Shown in Fig.3, in these cases, we only need to solve states in one side. There are six possible cases which are introduced in Section 3. Here we will use the example shown in Fig.3 to show how to solve the half Riemann problem.

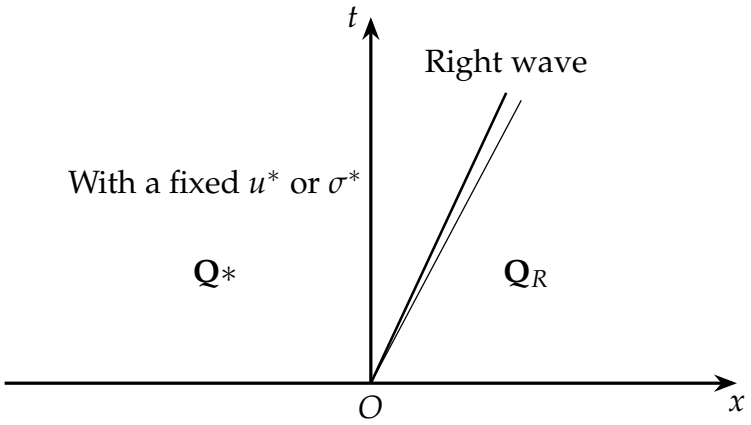

Figure 3: Half Riemann problem with a given left velocity or Cauchy stress.

As we know the velocity u^* or the Cauchy stress σ^* on one side, for example , the left side, there is only one equation need to be solved:

$$f(\rho^*, \mathbf{Q}_R) = u(\rho^*, \mathbf{Q}_R) - u^* = 0, \tag{5.1}$$

or

$$f(\rho^*, \mathbf{Q}_R) = \sigma(\rho^*, \mathbf{Q}_R) - \sigma^* = 0. \tag{5.2}$$

Similar to the process in Section (4.1), we have to use an iteration procedure to solve (5.1) or (5.2) and the solving process is list in the following.

Initial:

The initial density is given as

$$\rho^*_{(1)} = \rho_R. \tag{5.3}$$

Iterations begin:

Step 1 Determine the case of the wave structures:

Given the value of $\rho^*_{(k)}$ in the k-th iteration step, use the methods introduced in Section 4.2 to determine the case of wave structure of this Riemann problem. Here the subscript (k) means the variable in the k-th iteration step.

Step 2 Elevate $f(\rho^*, \mathbf{Q}_R)$:

After determining the structure case, evaluate the velocity (or the Cauchy stress) in the region $\mathbf{Q}^*$ and the details are given in Section 4.4.

Step 3 Evaluate the derivative of $f(\rho^*, \mathbf{Q}_R)$:

The derivative of f is given by

$$\frac{\partial f_{(k)}}{\partial \rho^*} = \frac{f_{(k)} - f_{(k-1)}}{\rho^*_{(k)} - \rho^*_{(k-1)}}, \text{ for } k > 1$$

At the first step,

$$\frac{\partial f_{(1)}}{\partial \rho^*} = \frac{f(\rho^* + \Delta\rho) - f(\rho^*)}{\Delta\rho},$$

where $\Delta\rho$ is a small quantity, here we set $\Delta\rho = \frac{\rho^*_{(1)}}{100}$.

Step 4 Evaluate $\rho^*_{(k+1)}$:

A new density can be updated by

$$\rho^*_{(k+1)} = \rho^*_{(k)} - f/\frac{\partial f_{(k)}}{\partial \rho}.$$

Step 5 Convergence test:

The iteration is convergent if

$$\text{CHA} \leq \text{TOL}, \tag{5.4}$$

where

$$\text{CHA} = \max\left[\frac{|\rho^*_{(k+1)} - \rho^*_{(k)}|}{\frac{1}{2}|\rho^*_{(k+1)} + \rho^*_{(k)}|}, |f|\right], \quad \text{TOL} = 10^{-4}.$$

If not, go to Step 1 and continue the iteration procedure until convergent. Numerical examples show, after 2-4 iterations, the condition (5.4) is satisfied.

Iterations end.

6. Numerical tests

In this section, by choosing different initial conditions, we will solve different Riemann problems with several different wave structures in the solutions. In order to verify the correctness of our exact Riemann solver, we use a third-order numerical scheme for 1D elastic-plastic flows introduced in [5] to evaluate these Riemann problems and compare numerical results with our exact solution.

In the following tests, the materials are taken as aluminium and copper. The parameters of the EOS and constitutive model for aluminum and copper are $(\rho_0, a_0, \Gamma_0, s, \mu)_{\text{Al}} = (8930\text{kg/m}^3, 3940\text{m/s}, 2, 1.49, 2.76, 2.76\times 10^{10}\text{Pa})$ and $(\rho_0, a_0, \Gamma_0, s, \mu)_{\text{copper}} = (2785\text{kg/m}^3, 5328\text{m/s}, 2, 1.338, 4.5\times 10^{10}\text{Pa})$, respectively. The yielding strengths of the two materials are $Y_{0,\text{Al}} = 3\times 10^8\text{Pa}$ and $Y_{0,\text{Copper}} = 9\times 10^7\text{Pa}$, respectively. The computational domain is seted as $[0, 1m]$ with 800 cell points and the intial interface is located at $0.5m$, the terminal time is $t = 5\times 10^{-5}s$. Otherwise, in the initial condition, "L" and "R" mean $x < 0.5m$ and $x > 0.5m$, respectively.

6.1. Test 1

In this case, the material is yielding at both sides, so there are three waves with two plastic shock waves and one contact. The initial condition is

$$\begin{cases} \text{L: Al}, \quad \rho = 2785\text{kg/m}^3, \quad u = 20\text{m/s}, \quad p = 1.0\text{Pa}, \quad s_{xx} = -2.0 \times 10^8\text{Pa}, \\ \text{R: Al}, \quad \rho = 2785\text{kg/m}^3, \quad u = 0\text{m/s}, \quad p = 1.0\text{Pa}, \quad s_{xx} = -2.0 \times 10^8\text{Pa}, \end{cases} \tag{6.1}$$

It can be seen that the exact solution matches the numerical results very well in Fig.4.

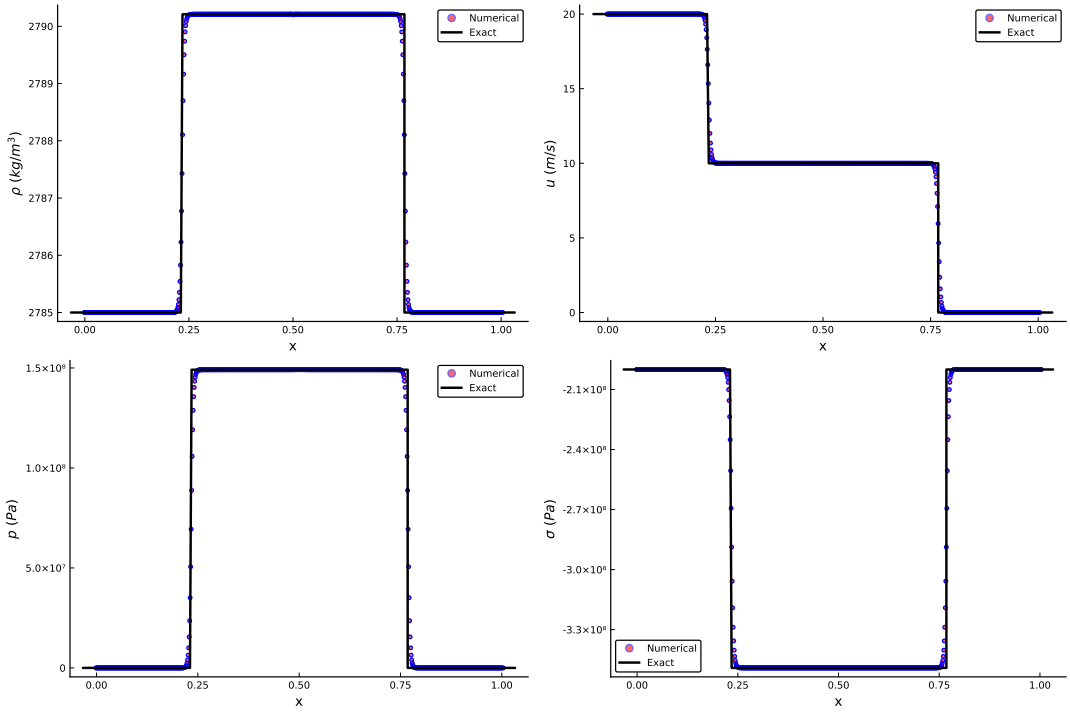

Figure 4: Comparison for Test 1 with the structure of $S^P|S^P$.

6.2. Test 2

Here we consider a case with yielding process at both sides, so there are five waves in the wave structure of this Riemann problem. The initial condition is

$$\begin{cases} \text{L: Al}, \quad \rho = 2785\text{kg/m}^3, \quad u = 800\text{m/s}, \quad p = 1.0\text{Pa}, \quad s_{xx} = 0.0\text{Pa}, \\ \text{R: Al}, \quad \rho = 2785\text{kg/m}^3, \quad u = 0\text{m/s}, \quad p = 1.0\text{Pa}, \quad s_{xx} = 0.0\text{Pa}, \end{cases} \tag{6.2}$$

Shown in Fig.5, the exact solution matches the numerical results well generally, except the under-cooling effect performed in the numerical results, but it is not considered in the designing of the exact Riemann solver.

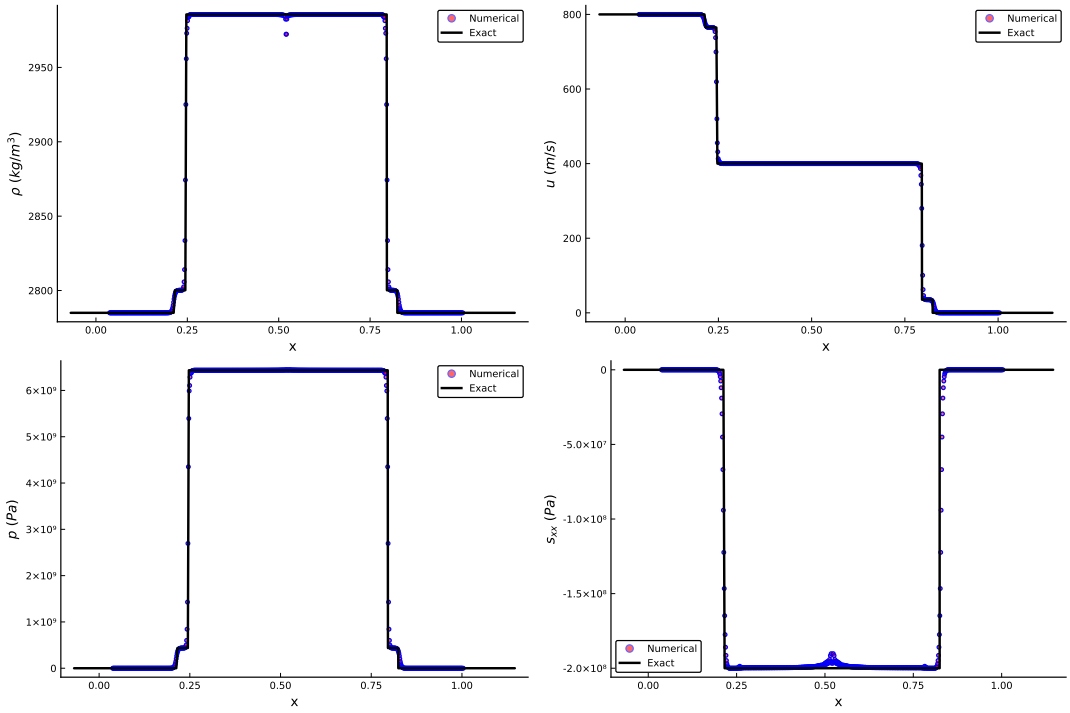

Figure 5: Comparison for Test 2 with the structure of $S^E S^P | S^P S^E$.

6.3. Test 3

In this example, we test the case with two elastic rarefaction waves. In the wave structure there is one elastic rarefaction wave on each side of the contact wave. The initial condition is given as

$$\begin{cases} \text{L: Al}, \quad \rho = 2785\text{kg/m}^3, \quad u = -2.0\text{m/s}, \quad p = 1.0^7\text{Pa}, \quad s_{xx} = 0.0\text{Pa}, \\ \text{R: Al}, \quad \rho = 2785\text{kg/m}^3, \quad u = 2.0\text{m/s}, \quad p = 1.0 \times 10^7\text{Pa}, \quad s_{xx} = 0.0\text{Pa}, \end{cases} \tag{6.3}$$

We can see that the results of the exact solution match the numerical results very well.

6.4. Test 4

In this test we test the example with both elastic and plastic rarefaction waves on both sides of contact wave. The initial condition is

$$\begin{cases} \text{L: Al}, \quad \rho = 2785\text{kg/m}^3, \quad u = -40\text{m/s}, \quad p = 1.0 \times 10^7\text{Pa}, \quad s_{xx} = 0.0\text{Pa}, \\ \text{R: Al}, \quad \rho = 2785\text{kg/m}^3, \quad u = 40\text{m/s}, \quad p = 1.0 \times 10^7\text{Pa}, \quad s_{xx} = 0.0\text{Pa}. \end{cases} \tag{6.4}$$

Results are shown in Fig.7, the results of the exact solver match the numerical results very well.

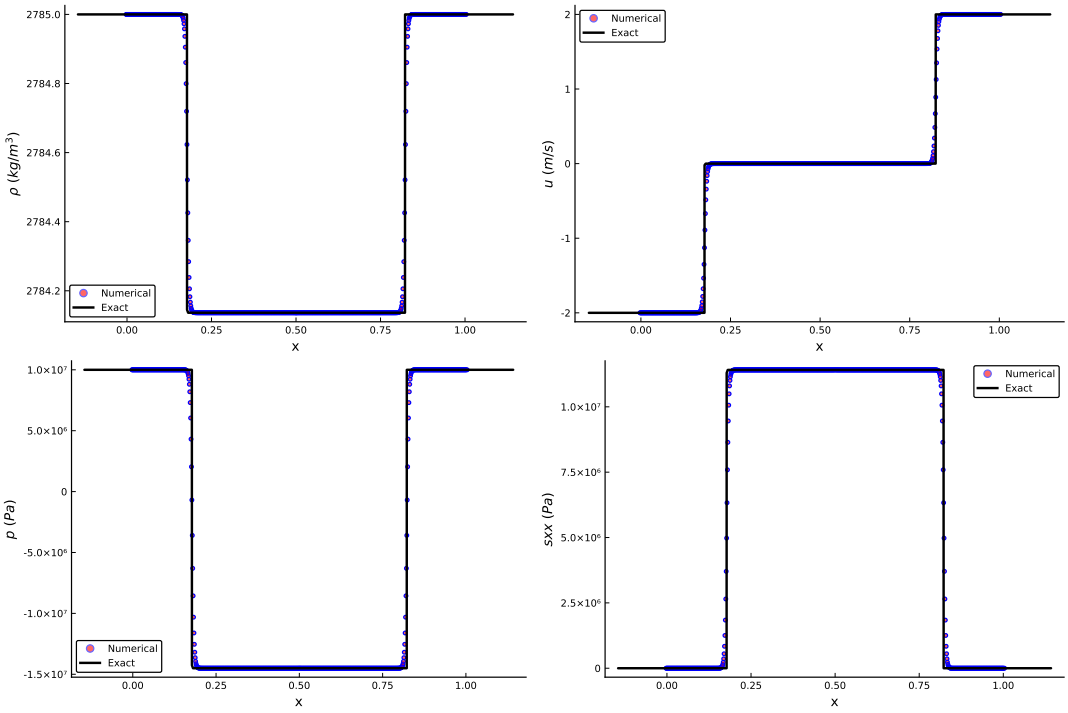

Figure 6: Comparison results for Test 3 with the wave structures of $R^E|R^E$.

6.5. Test 5

The initial condition of this Riemann problem is

$$\begin{cases} \text{L: Al}, \quad \rho = 2785\text{kg/m}^3, \quad u = -200\text{m/s}, \quad p = 1.0\text{Pa}, \quad s_{xx} = -2.0^8\text{Pa}, \\ \text{R: Al}, \quad \rho = 2785\text{kg/m}^3, \quad u = 0\text{m/s}, \quad p = 1.0\text{Pa}, \quad s_{xx} = -2.0^8\text{Pa}. \end{cases} \tag{6.5}$$

Obviously, at the beginning, the material is in the negative plastic state (i.e. $s_{xxL(R)} = -\frac{2}{3}Y^0$). According to the analysis introduced in Section 3.3, after an expanding process the material will turn back into an elastic state and will yield again into a positive plastic state. Our exact solution in Fig.8 are constitent with the analysis in Section 3.3. Of course, our exact solution matches the numerical solutions very well.

6.6. Test 6

The initial condition of this Riemann problem is

$$\begin{cases} \text{L: Al}, \quad \rho = 2785\text{kg/m}^3, \quad u = 200\text{m/s}, \quad p = 1.0\text{Pa}, \quad s_{xx} = 2.0^8\text{Pa}, \\ \text{R: Al}, \quad \rho = 2785\text{kg/m}^3, \quad u = 0\text{m/s}, \quad p = 1.0\text{Pa}, \quad s_{xx} = 2.0^8\text{Pa}. \end{cases} \tag{6.6}$$

Different from Test 5, at the beginning, the material is in the positive plastic state (i.e. $s_{xxL(R)} = \frac{2}{3}Y^0$). According to the analysis introduced in Section 3.3, after an compressing process the material will turn back into an elastic state and will yield again into a negtive plastic state. We can get the exact solutions which match the numerical solutions very well in Fig.9.

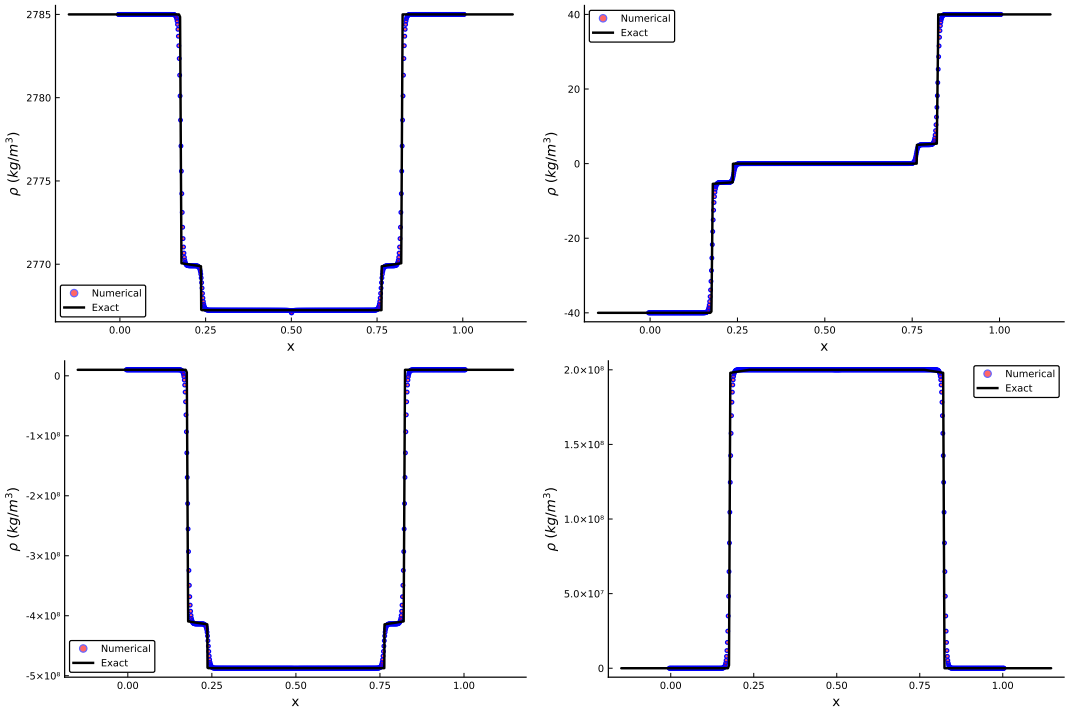

Figure 7: Comparison for Test 4 with the wave structure of $R^E R^P | R^P R^E$.

6.7. Test 7

All the above five tests have symmetrical wave structures. Here we will test an example with different structures on two sides: one plastic shock on the left side and both the elastic shock and plastic shock on the right side of one contact wave. The initial condition is given as

$$\begin{cases} \text{L: Al}, \quad \rho = 2785\text{kg/m}^3, \quad u = 40\text{m/s}, \quad p = 1.0 \times 10^8\text{Pa}, \quad s_{xx} = -2.0 \times 10^8\text{Pa}, \\ \text{R: Al}, \quad \rho = 2785\text{kg/m}^3, \quad u = -40\text{m/s}, \quad p = 1.0 \times 10^2\text{Pa}, \quad s_{xx} = 0.0\text{Pa}. \end{cases} \tag{6.7}$$

The solutions of this test are shown in Fig.10. From this figure, we can find the exact solutions match numerical solutions very well.

6.8. Test 8

In this test, we consider an example with zero initial velocities on both sides, driving by the gradient of the pressure, there are rarefaction waves produced into the higher pressure side and shock waves generated into the lower pressure side. The initial condition is given as

$$\begin{cases} \text{L: Al}, \quad \rho = 2785\text{kg/m}^3, \quad u = 0.0\text{m/s}, \quad p = 1.0 \times 10^{10}\text{Pa}, \quad s_{xx} = 0.0\text{Pa}, \\ \text{R: Al}, \quad \rho = 2785\text{kg/m}^3, \quad u = 0.0\text{m/s}, \quad p = 1.0 \times 10^2\text{Pa}, \quad s_{xx} = 0.0\text{Pa}. \end{cases} \tag{6.8}$$

Shown in Fig.14, we can see there are two shocks in the right side and two rarefaction waves on the left side.

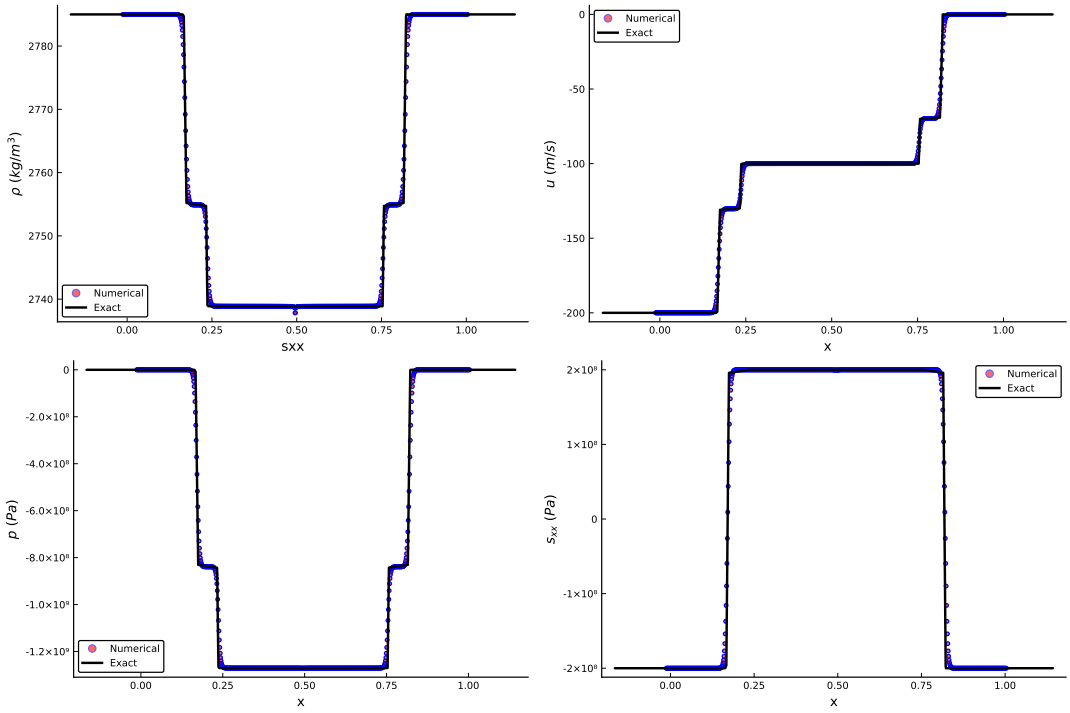

Figure 8: Comparison results for Test 5 with the structure of $R^E R^P | R^P R^E$.

6.9. Test 9

Now we will consider two multi-material tests with different materials on both sides. In this test, on the left side, the lighter material of aluminum impacts the heavier material of Copper. The initial condition is given as

$$\begin{cases} \text{L: Al}, \quad \rho = 2785\text{kg/m}^3, \quad u = 40\text{m/s}, \quad p = 0.1\text{Pa}, \quad s_{xx} = 0.0\text{Pa}, \\ \text{R: Copper}, \quad \rho = 8930\text{kg/m}^3, \quad u = 0.0\text{m/s}, \quad p = 0.1\text{Pa}, \quad s_{xx} = 0.0\text{Pa}. \end{cases} \tag{6.9}$$

Shown in the Fig.12, there is a large jump of density at the material interface and both the elastic shock and the plastic shock exist in each side of the interface. Comparing with the numerical results of the scheme with MHLLCEP approximate solver, we can find that our exact Riemann solver can solve the Riemann problem with multi-materials very well.

6.10. Test 10

Here we test another multi-materials case. In this test the initial condition is given as

$$\begin{cases} \text{L: Copper}, \quad \rho = 8930\text{kg/m}^3, \quad u = 0.0\text{m/s}, \quad p = 1.0 \times 10^{10}\text{Pa}, \quad s_{xx} = 0.0\text{Pa}, \\ \text{R: Al}, \quad \rho = 2785\text{kg/m}^3, \quad u = 0\text{m/s}, \quad p = 10.0\text{Pa}, \quad s_{xx} = 0.0\text{Pa}. \end{cases} \tag{6.10}$$

Shown in Fig.13, there are two rarefaction waves on the left side and two shocks on the right side. Moreover, we can find that there is the discontinuity of pressure on the interface, and the Cauchy stress is continuous, which satisfies the theoretical analysis.

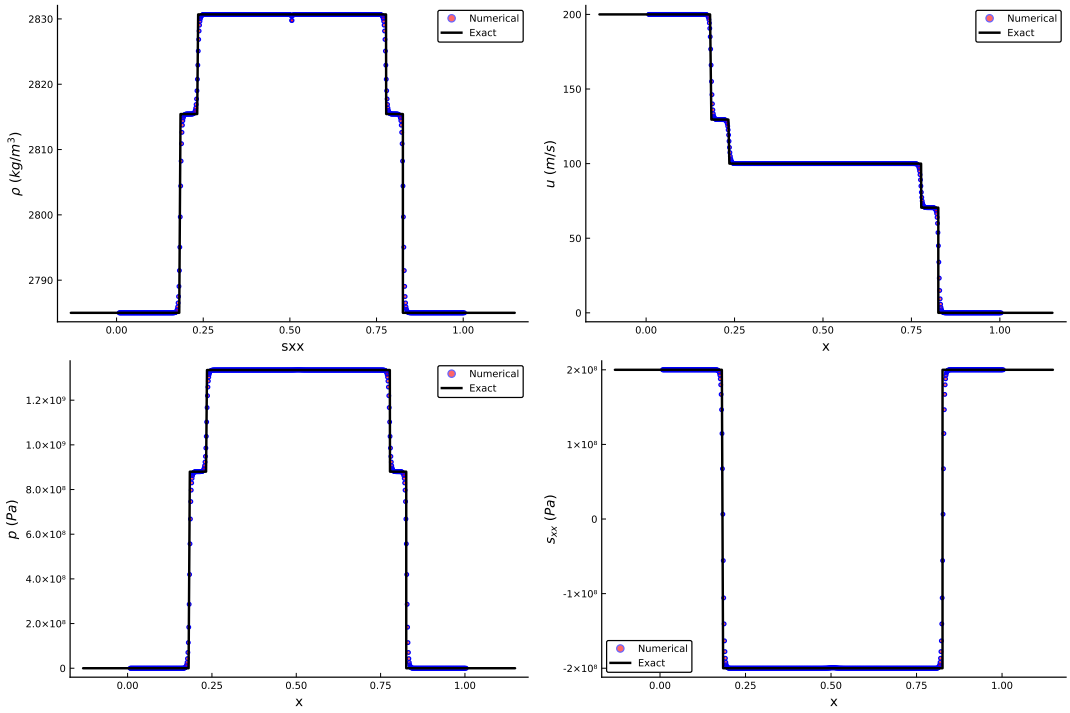

Figure 9: Comparison results for Test 6 with the structure of $S^E S^P | S^P S^E$.

6.11. Test 11

This test is the half Riemann problem with a given velocity $u^* = -20\text{m/s}$ on the left, and the right initial condition is

$$\text{Copper}, \quad \rho = 8930\text{kg/m}^3, \quad u = 0.0\text{m/s}, \quad p = 0.1\text{Pa}, \quad s_{xx} = 0.0\text{Pa}. \tag{6.11}$$

In Fig.14, comparison results are given by the exact half Riemann solver and the numerical method. We can see that the exact solver can resolve both the elastic shock and the plastic shock wave very well.

6.12. Test 12

The second half Riemann case is with a given Cauchy stress $\sigma^* = 0\text{Pa}$ on the left, and the right initial condition is

$$\text{Copper}, \quad \rho = 8930\text{kg/m}^3, \quad u = 0.0\text{m/s}, \quad p = 1.0 \times 10^9\text{Pa}, \quad s_{xx} = 0.0\text{Pa}. \tag{6.12}$$

In Fig.15, we give the results computed by the exact Riemann solver and the numerical simulation. From this figure one can see, the exact solver can resolve the elastic and plastic rarefaction waves well.

7. Results

In this paper, we have detailedly analyzed the Riemann problem for one-dimensional multi-material elastic-plastic flows with the Mie-Grüneisen EOS, hypo-elastic constitutive model and the von Mises' yielding condition and found

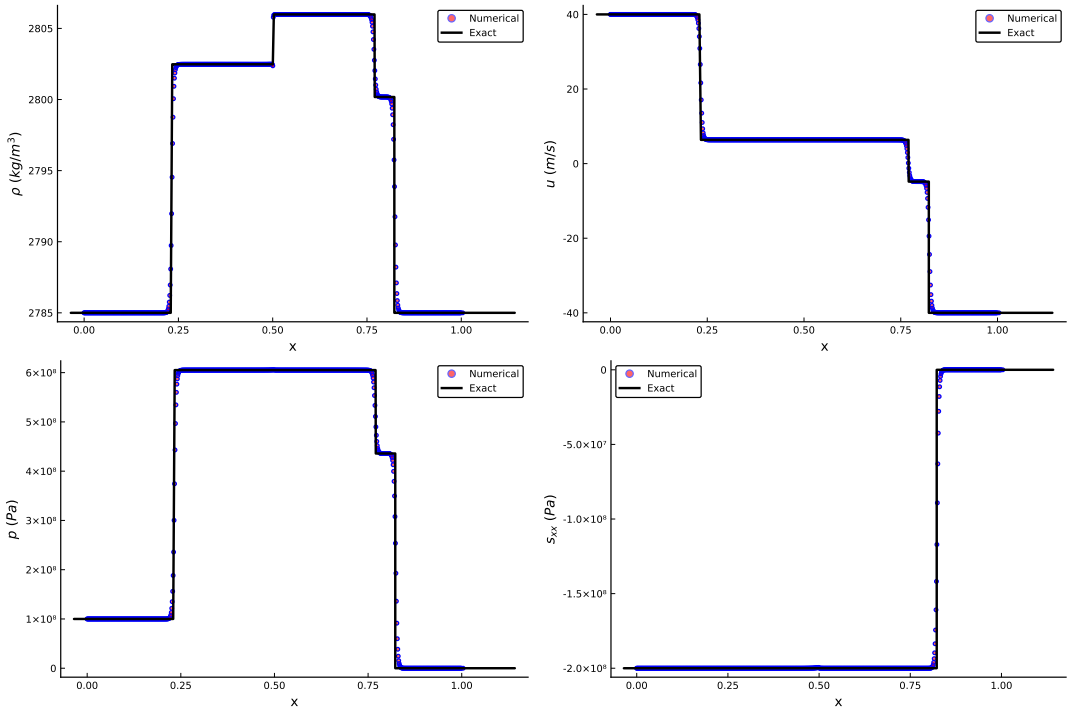

Figure 10: Comparison resutls for Test 7 with the structure of $R^P|R^P R^E$.

1. The sonic speed periods a significant jump when the material is yielding.
2. the plastic wave is always faster than the elastic wave for the reason of the sonic speed jump.
3. There are only thirty-six possible cases of the wave structure in the Riemann problem.
4. All the variables after the non-linear waves can be written as functions of the density theoretically.
5. If the initial material is in the negative plastic state, after being expanded, the material may be into the elastic state or the positive plastic state and vice versa.

Then, based on the above analysis, we have constructed exact Riemann solvers for both the Riemann problem and the half Riemann problem, separately. Tested by a large number of examples, the exact Riemann solver is reasonable and its solutions are matching well with the numerical results for both single material problems and multi-material Riemann problems.

Acknowledgement

This work was supported by NSFC(Grant No. 11672047) and Science Challenge Project (Grant No. TZ2016002).

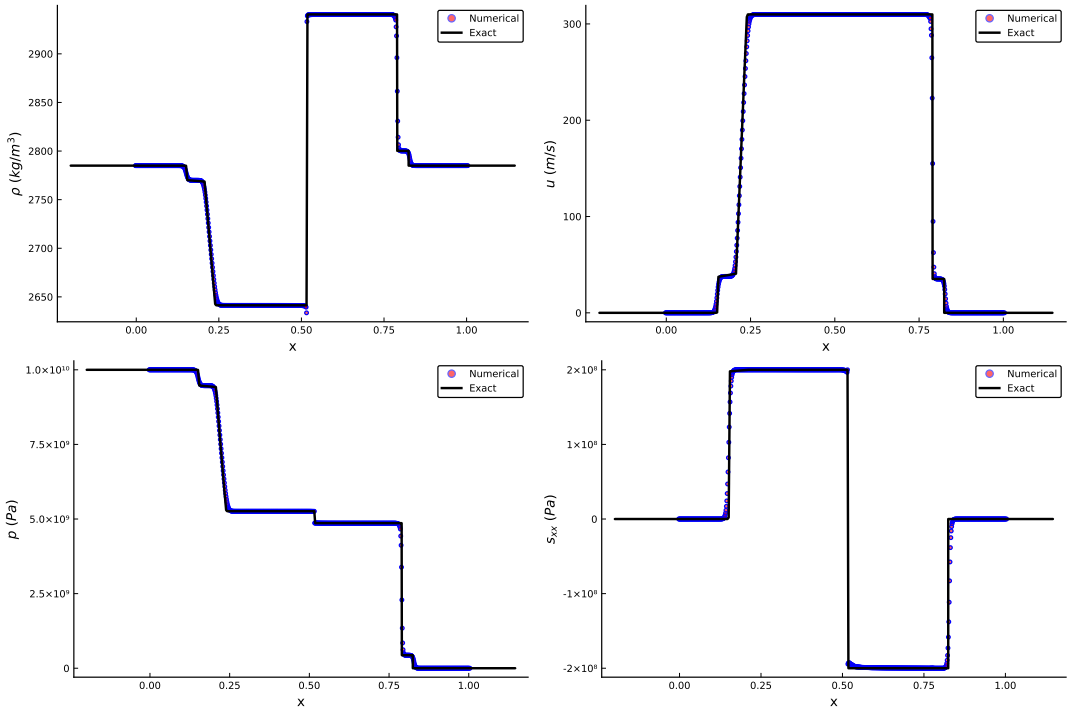

Figure 11: Comparison resutls for Test 8 with the structure of $R^E R^P | S^P S^E$.

References

[1] M. L. Wilkins, Calculation of elastic-plastic flow, Tech. rep., California Univ Livermore Radiation Lab (1963).

[2] S. L. Gavrilyuk, N. Favrie, R. Saurel, Modelling wave dynamics of compressible elastic materials, Journal of computational physics 227 (5) (2008) 2941–2969.

[3] J.-B. Cheng, E. F. Toro, S. Jiang, M. Yu, W. Tang, A high-order cell-centered Lagrangian scheme for one-dimensional elastic–plastic problems, Computers & Fluids 122 (2015) 136–152.

[4] J. Cheng, Harten-Lax-van Leer-contact (HLLC) approximation Riemann solver with elastic waves for one-dimensional elastic-plastic problems, Applied Mathematics and Mechanics 37 (11) (2016) 1517–1538.

[5] L. Liu, J.-b. Cheng, A multi-material HLLC Riemann solver with both elastic and plastic waves for 1D elastic-plastic flows, https://www.researchgate.net/publication/332709456_A_multi-material_HLLC_Riemann_solver_with_both_elastic_and_plastic_waves_for_1D_elastic-plastic_flows, (preprint).

[6] X. Garaizar, Solution of a Riemann problem for elasticity, Journal of elasticity 26 (1) (1991) 43–63.

[7] G. H. Miller, An iterative Riemann solver for systems of hyperbolic conservation laws, with application to hyperelastic solid mechanics, Journal of Computational Physics 193 (1) (2004) 198–225.

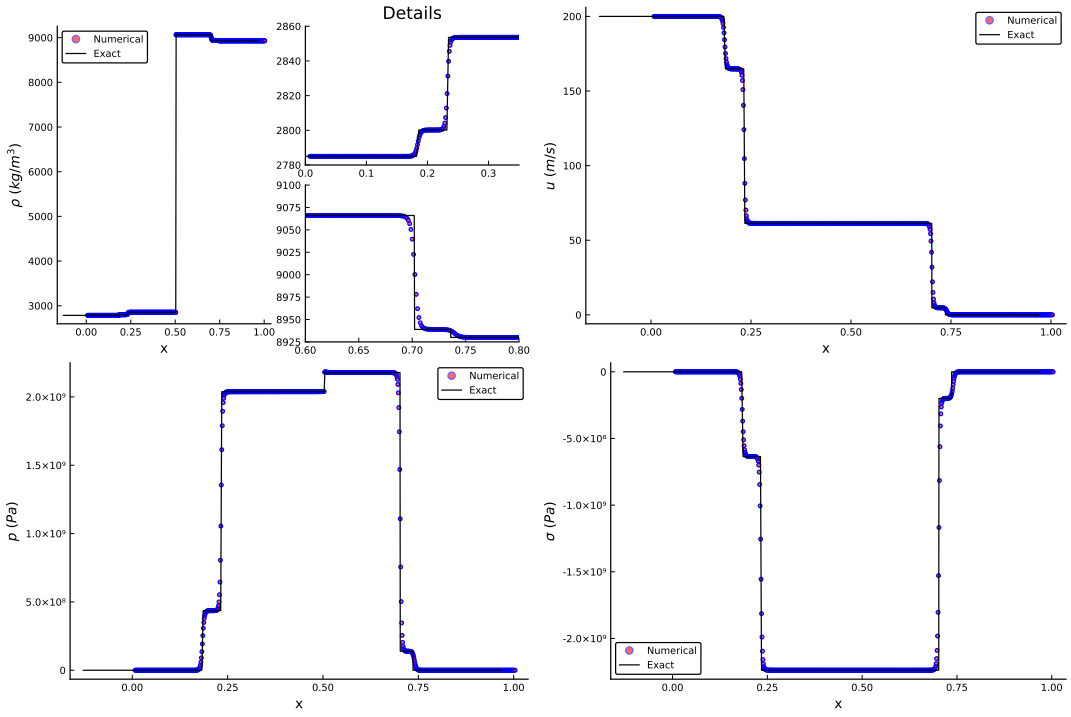

Figure 12: Comparison results for Test 9 with the structure of $R^E R^P | R^P R^E$.

[8] S. Gao, T. Liu, 1d exact elastic-perfectly plastic solid Riemann solver and its multi-material application, Advances in Applied Mathematics and Mechanics 9 (3) (2017) 621–650.

[9] S. Gao, T. Liu, C. Yao, A complete list of exact solutions for one-dimensional elastic-perfectly plastic solid Riemann problem without vacuum, Communications in Nonlinear Science and Numerical Simulation 63 (2018) 205–227.

[10] A. L. Ortega, M. Lombardini, D. Pullin, D. I. Meiron, Numerical simulation of elastic–plastic solid mechanics using an Eulerian stretch tensor approach and HLLD Riemann solver, Journal of Computational Physics 257 (2014) 414–441.

[11] N. Favrie, S. Gavrilyuk, Dynamics of shock waves in elastic-plastic solids, in: ESAIM: Proceedings, Vol. 33, EDP Sciences, 2011, pp. 50–67.

[12] P.-H. Maire, R. Abgrall, J. Breil, R. LoubèRe, B. Rebourcet, A nominally second-order cell-centered Lagrangian scheme for simulating elastic–plastic flows on two-dimensional unstructured grids, Journal of Computational Physics 235 (2013) 626–665.

A. Numerical intergration for the rarefaction wave

There are two integrations in functions $p(\rho)$ and $u(\rho)$ in the rarefaction wave, for example, in the equations (4.14) and (4.15). In this paper, we use a seventh-order (with 4 integrating points) Gaussian quadrature to

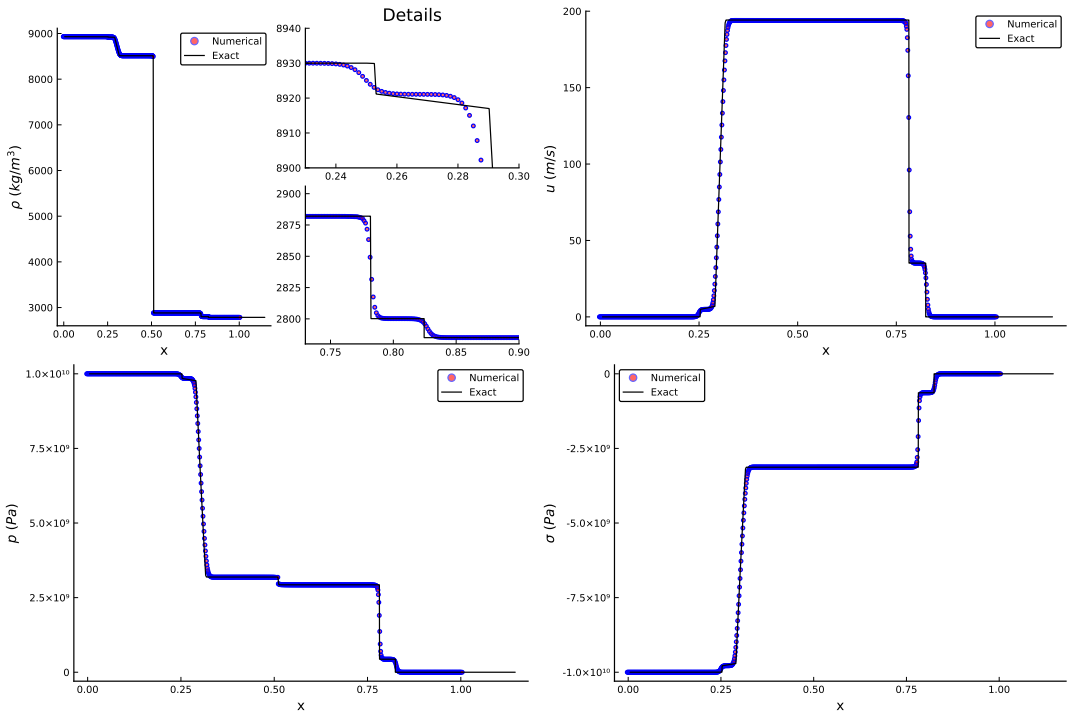

Figure 13: Comparison results for Test 10 with the structure of $R^E R^P | S^E S^P$.

make numerical integrations. For a function $g(x)$, the Gaussian integration from -1 to 1 is given as

$$\int_{-1}^{1} g(x)dx \approx \sum_{i=1}^{n} \omega_i g(x_i),$$

ω_i is the weight, and x_i is the integrating point, n is the number of the Gaussian quadrature points. Here $n = 4$. For the 7th-order Gaussian quadrature, integrating points and corresponding weights are

$$x_1,\ x_2 = \pm\sqrt{\frac{3}{7} - \frac{2}{7}\sqrt{\frac{6}{5}}} \quad \left(\omega_1,\ \omega_2 = \frac{18+\sqrt{30}}{36}\right),$$

$$x_3,\ x_4 = \pm\sqrt{\frac{3}{7} + \frac{2}{7}\sqrt{\frac{6}{5}}} \quad \left(\omega_3,\ \omega_4 = \frac{18-\sqrt{30}}{36}\right).$$

For the function $g(x)$ over $[\rho_0, \rho]$, this change of interval can be done in the following way:

$$\int_{\rho_0}^{\rho} g(x)dx = \frac{\rho-\rho_0}{2}\int_{-1}^{1} g\left(\frac{\rho-\rho_0}{2}x + \frac{\rho_0+\rho}{2}\right)dx.$$

At last, we can get

$$\int_{\rho_0}^{\rho} g(x)dx \approx \frac{\rho-\rho_0}{2}\sum_{i=1}^{n}\omega_i g\left(\frac{\rho-\rho_0}{2}x_i + \frac{\rho_0+\rho}{2}\right). \tag{A.1}$$

Integrating of $p(\rho)$

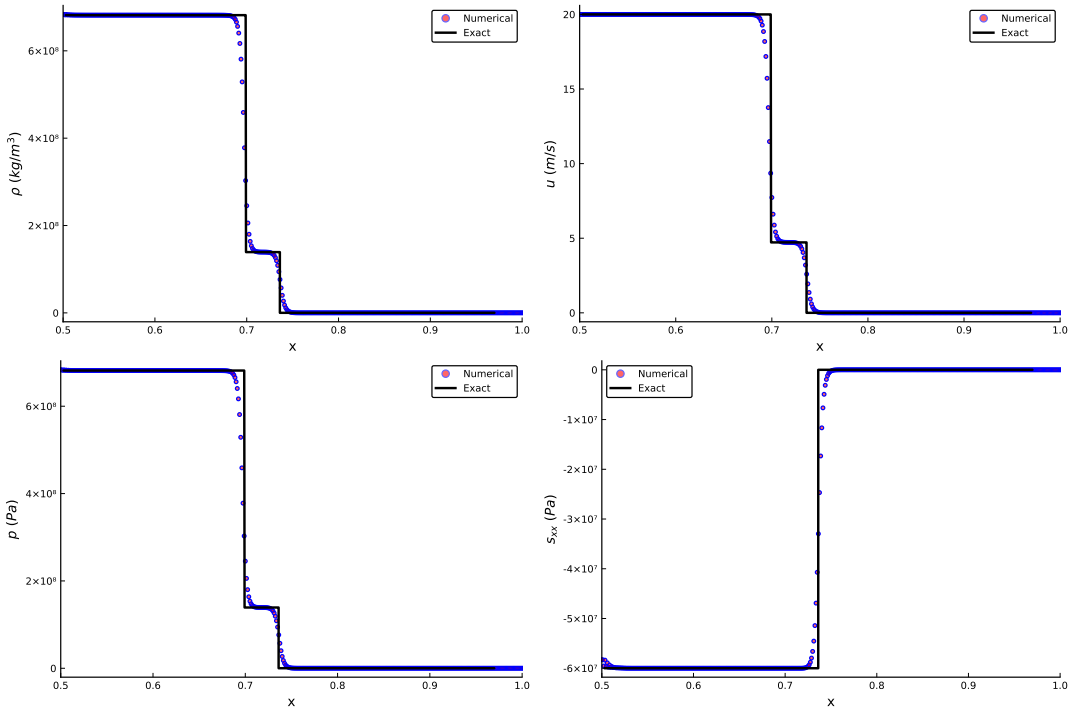

Figure 14: Comparison results for Test 11 with the structure of $S^E S^P$.

Taking Equation (4.14) as an example,

$$p(\rho) \approx p_{L(R)} e^{\frac{\lambda}{\rho_{L(R)}} - \frac{\lambda}{\rho}} + e^{-\frac{\lambda}{\rho}} \mathrm{Intg}_1, \tag{A.2}$$

where

$$\mathrm{Intg}_1 = \frac{\rho - \rho_{L(R)}}{2} \sum_{n=1}^{4} \omega_i f_2(\rho_i) e^{\lambda/\rho_i},$$

and $\rho_i = \frac{\rho - \rho_{L(R)}}{2} x_i + \frac{\rho_{L(R)} + \rho}{2}$.

Obviously, we can use (A.2) to evaluate all the values of $p(\rho_i)$ on all Gaussian quadrature points.

Integrating of $u(\rho)$

Taking Equation (4.15) as an example, if the wave is on the left side

$$u(\rho) = u_L - \int_{\rho_L}^{\rho} \frac{c_e(x)}{x} dx.$$

The numerical integration of $u(\rho)$ is given as

$$u(\rho) \approx u_L - \mathrm{Intg}_2 \tag{A.3}$$

where

$$\mathrm{Intg}_2 = \frac{\rho - \rho_{L(R)}}{2} \sum_{n=1}^{4} \omega_i \frac{c_e(\rho_i)}{\rho_i},$$

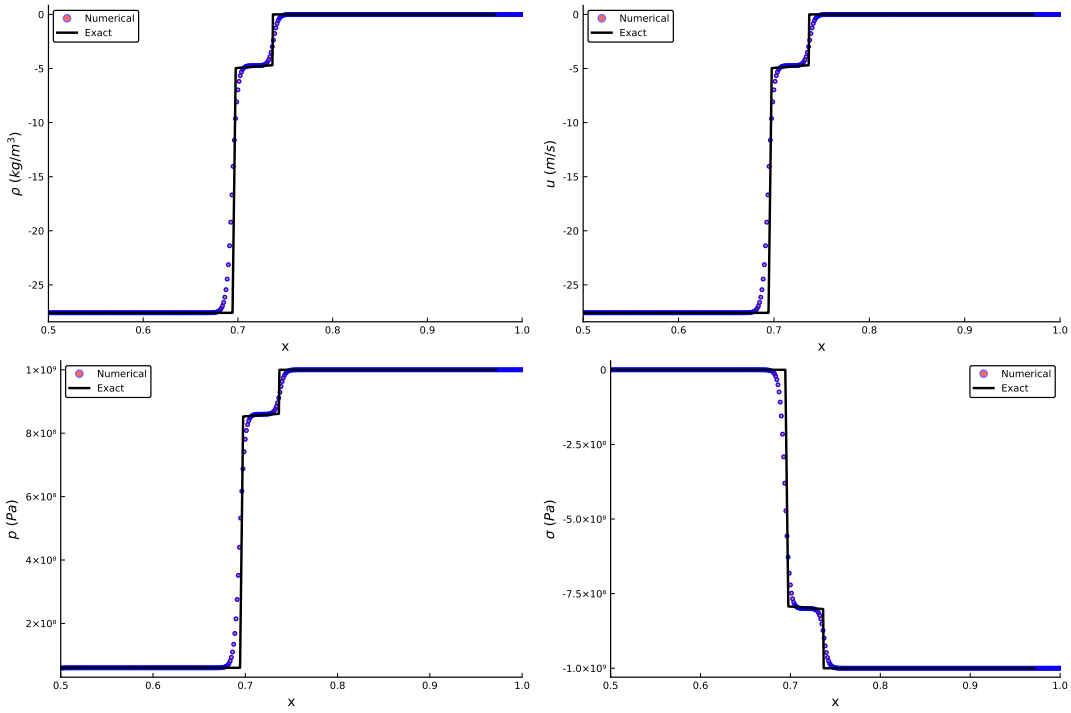

Figure 15: Comparison results for Test 11 with the structure of $R^E R^P$.

Different from (A.2), the sonic speed $c_e(\rho_i)$ is dependent on $p(\rho_i)$:

$$c_e(\rho_i) = \sqrt{a_0^2 \frac{\partial f}{\partial \eta}\left(\frac{\rho_i}{\rho_0}\right) + \frac{p(\rho_i)}{\rho_i^2}\rho_0\Gamma_0 - \frac{\rho_0}{\rho_i^2}\Gamma_0 s_{xx}(\rho_i) + \frac{4}{3}\frac{\mu}{\rho_i}}. \tag{A.4}$$

After finishing the evaluation of $p(\rho_i)$, we can evaluate $c_e(\rho_i)$ by using the same process as (A.2).